Mbnl1 knockout mice manifest some DM-like phenotypes such as myotonia, cataracts and splicing misregulation, whereas overexpression of Mbnl1 in DM model mice ameliorates the disease phenotypes (13–15). MBNL2 also accumulates in RNA foci in DM tissues, and *Mbnl2* knockout mice exhibit myotonia or brain abnormalities including sleep disorder and learning deficits (10,16,17). Therefore, MBNL proteins are recognized as key mediators, in addition to pathological molecular markers, of repeat expansion diseases such as DM1.

One major class of coding repeat expansion diseases is CAG-repeat diseases, which include Huntington's disease (HD). An expansion of CAG repeats encoding a polyglutamine (polyQ) tract leads to production of an aggregation-prone protein with various toxic effects (18). Although coding CAG-repeat diseases and non-coding CTG repeat diseases have been attributed to protein and RNA gain-of-function mechanisms, respectively, recent studies have revealed overlapping features between these diseases. CAG-repeat-containing transcripts are expressed from the disease allele and produce polyQ-containing proteins in DM1, SCA8 and HDL2 (19–21), whereas toxic effects of CAG-repeat RNA have been suggested in polyQ diseases (22–25). Furthermore, a recent study reports that expanded-repeat RNA can be translated even without an ATG codon (21). In this process, RAN translation, a single repeat tract can produce homopolymeric proteins in multiple frames (21). Thus, gene products from an expanded allele are much more complex than previously recognized. Interestingly, MBNL1 binds to CAG repeats in addition to CUG and CCUG repeats and accumulates in CAG-repeat RNA foci (9,26,27). In addition, MBNL1 and its orthologs can modulate the toxicity of the CAG repeat in animal models (22,25). Thus, MBNL proteins have become potential common players in many repeat expansion diseases, not only CTG/CCTG repeat diseases.

A key issue related to both the abnormal regulation and function of MBNL1 in repeat expansion diseases is the alternative splicing of exon 7 in this protein. The inclusion of this exon is elevated in DM1, DM2 and SCA8 patients and model mice (8,11,28). Moreover, the same alteration is observed in $Mbnl1^{\Delta ex3/\Delta ex3}$ knockout mice, suggesting an autoregulation of exon 7 by MBNL1 (11,29). Furthermore, isoforms containing this exon exhibit nuclear localization (11,30,31), although the mechanism of nuclear localization of MBNL1 is still elusive. Another key issue related to MBNL1 in the nucleus is the precise effect of the RNA foci formation. As demonstrated in DM pathogenesis, nuclear interaction between MBNL proteins and mutant RNA leads to loss of MBNL function. However, it is still unclear whether the colocalization of MBNL1 and repeat RNA in the inclusions reflects some active response of MBNL1 or a passive sequestration of MBNL1. Indeed, recent studies have shown that depletion of MBNL1 reduces ribonuclear inclusions (32–34), supporting the notion that MBNL1 is involved in the process of foci formation.

In this study, we investigated the mechanism, regulation and significance of MBNL1 nuclear localization. We found that nuclear localization is a major determinant of MBNL1 function. We then focused on the regulation of nuclear localization of MBNL1 and identified novel conserved motifs that cooperatively mediate nuclear localization of MBNL1. Alternative splicing of exon 7 acts as a regulatory switch that couples MBNL1 nuclear activity and nuclear localization. Finally, we identified the significance of the interaction between MBNL1 protein and repeat RNA in the nucleus. MBNL1 promotes the nuclear retention of repeat-containing transcripts, which results in repression of aberrant protein expression from the expanded repeats, pointing to a novel aspect of RNA foci formation as well as a potential strategy for preventing protein toxicity in repeat expansion diseases.

RESULTS

Intracellular localization of MBNL isoforms

Mammalian MBNL proteins show complex splicing variations (Fig. 1A and Supplementary Material, Fig. S1A). We first tried to identify the determinants of MBNL1 properties in relation to splice variations. In this study, subcellular localization of protein or RNA was evaluated by automated fluorescence analysis of individual transfected cells (35). The nucleocytoplasmic index (NCI) ranges from 0 to 1 with higher values indicating stronger cytoplasmic localization in a cell. An averaged NCI value from a cell population was used as a representative value of the transfected construct. Using this system, intracellular localization of EGFP-fused MBNL1 isoforms was analyzed in comparison with the control, EGFP. In COS-7 cells, only $MBNL1_{42}$ showed nuclear localization (Fig. 1B and C). Thus, exon 7, which is included only in this isoform, must be involved in nuclear localization (Fig. 1A). The other isoforms showed more cytoplasm localization with $MBNL1_{40s}$ showing the most cytoplasmic localization (Fig. 1B and C). Protein expression of these isoforms was verified by western blot (Supplementary Material, Fig. S1C). We also confirmed that C-terminally myc-tagged MBNL1 isoforms showed subcellular localization similar to that of N-terminally EGFP-tagged ones (Supplementary Material, Fig. S5C).

Next, we compared splicing regulatory activity of these isoforms using an *Actn1* minigene (36,37). This minigene contains two mutually exclusive alternative exons, NM (non-muscle) and SM (smooth muscle) (Fig. 1D). In the basal splicing pattern, NM inclusion was predominant. When the amount of MBNL1 was increased, NM inclusion was gradually reduced, whereas SM inclusion was transiently increased and then decreased at maximum MBNL1 dose (Fig. 1D). Among MBNL1 isoforms, $MBNL1_{42}$ had the strongest effect on *Actn1* splicing (Fig. 1E), consistent with its strong nuclear localization. Isoforms 41, 40, 41 and 40s exhibited *Actn1* splicing regulation weaker than that of $MBNL1_{42}$ but stronger than isoforms 36 and 35 (Fig. 1E and Supplementary Material, Fig. S1D). Both $MBNL1_{36}$ and $MBNL1_{35}$ lacked exon 5 (Fig. 1A), suggesting that the linker region between ZnF1/2 and ZnF3/4 encoded by this exon determines the splicing regulatory activity of MBNL1. An N-terminal region of MBNL1 with four ZnF motifs (MBNL1-N) alone showed much weaker activity compared with $MBNL1_{42}$ (Fig. 1F). This reduction can be explained by its weaker nuclear localization (Fig. 1C); the activity of MBNL1-N splicing regulation was fully recovered by the addition of an NLS, whereas it was further reduced by the addition of a nuclear export signal (NES) (Fig. 1C and F). The regulatory activity of MBNL1-N was weakened when exon 5 was deleted (Fig. 1F, MBNL1-NΔex5). However, the presence of exon 5 is not an absolute requirement for splicing regulation, as

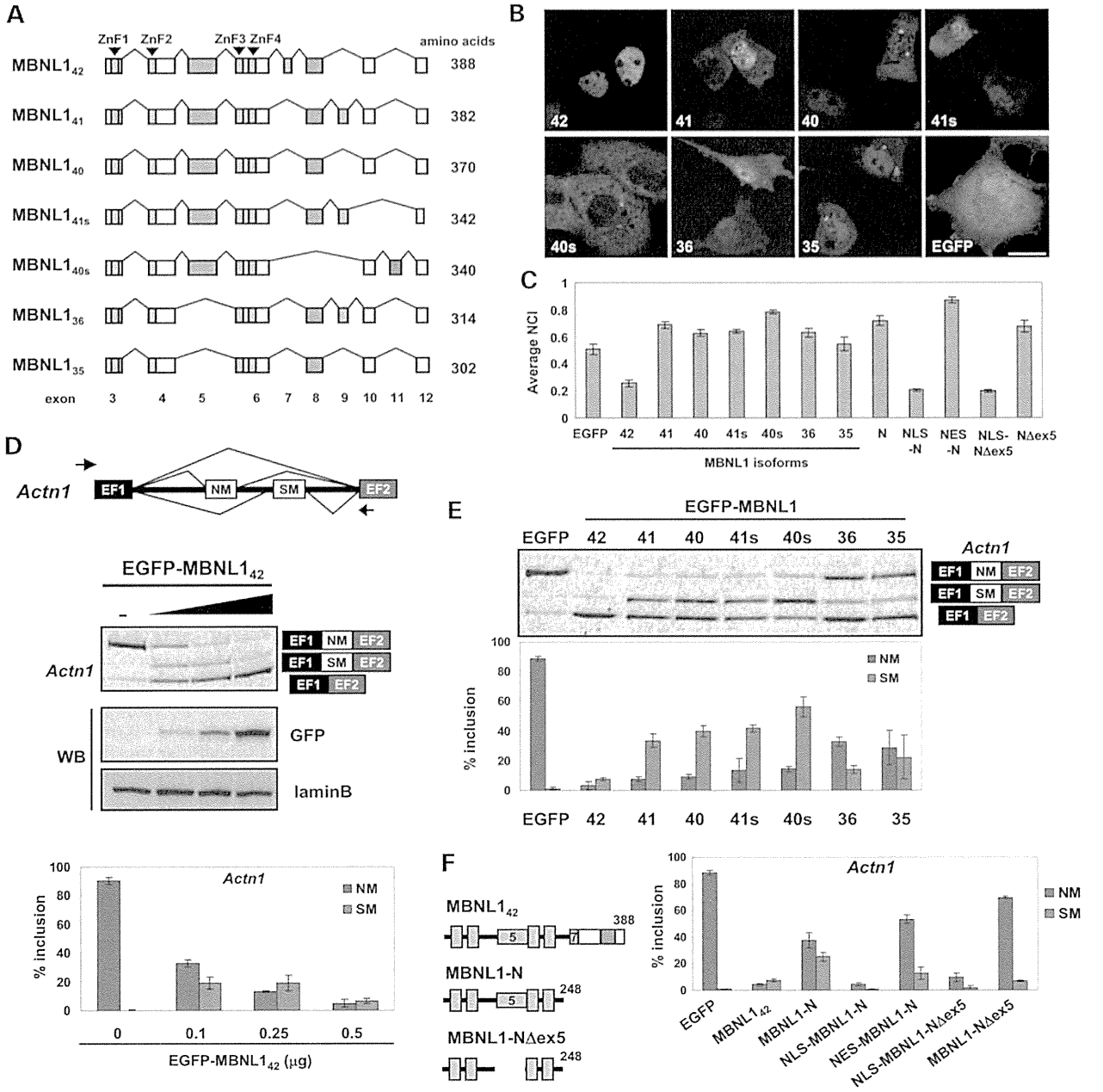

Figure 1. Splice variation in MBNL proteins. (**A**) Structures of MBNL isoforms. Alternative exons (5, 7, 8, 9, 10 and 11) are indicated by different colors. Blue boxes indicate zinc finger motifs. (**B**) Intracellular localization of MBNL isoforms. The expression of EGFP-fused MBNL isoforms in COS-7 cells was observed by confocal microscopy. Hoechst 33342 was used to stain the nucleus. Scale bar represents 20 μm. (**C**) Quantitative localization analysis of EGFP-fused MBNL1 isoforms. Bars indicate average NCI value (see text) of transformants in COS-7 cells. EGFP serves as a control. (**D**) Dose-dependent splicing regulation of *Actn1* minigenes by EGFP-MBNL1$_{42}$ in COS-7 cells. Structure of *Actn1* minigenes is shown at the top. Arrows indicate the position of primers used in the splicing assays. The results of splicing assay of *Actn1* and western blots of EGFP-MBNL1 and endogenous Lamin B are shown in the middle panels. Bar chart shows the quantified results of *Actn1* splicing assay (mean ± SD, $n = 3$). (**E**) Splicing regulation of *Actn1* by EGFP-fused MBNL1 isoforms in COS-7 cells. Bar chart shows quantified results (mean ± SD, $n = 3$). (**F**) *Actn1* splicing assay of the N-terminal region of MBNL1 in COS-7 cells. An NLS or NES-fused MBNL1-N was also examined. NΔex5 is a common N-terminus region of MBNL1$_{35}$ and MBNL1$_{36}$. Bar chart shows quantified results as in (E).

NLS-fused NΔex5 showed splicing regulation similar to that of MBNL1$_{42}$ or NLS-MBNL1-N (Fig. 1F). In conclusion, the splicing regulatory activity of MBNL1 can be attributed to the N-terminus region containing four ZnF motifs and a linker region, although the activity is also determined by the degree of nuclear localization that is mediated by the C-terminus including exon 7. Similarly, MBNL2 has an alternative exon corresponding to MBNL1 exon 7, which is associated with nuclear localization and stronger splicing regulation (Supplementary Material, Fig. S2A–C).

Identification of a nuclear localization signal in the C-terminus of MBNL1

As seen earlier, nuclear localization is a major determinant for the functions of MBNL1. We sought to identify the mechanism of its nuclear localization using EGFP-fused MBNL1 mutants. In both COS-7 and Neuro2a (N2a) cells, a C-terminal region of $MBNL1_{42}$ was essential for nuclear localization, as the deletion of the C-terminus disrupted nuclear localization (1–248, Fig. 2A). In addition, the C-terminus of $MBNL1_{42}$ (C42), but not of the other isoforms (C40. C41, C40s and C41s), was sufficient for inducing nuclear localization (Fig. 2A). Deletion analysis of this region revealed that nuclear localization activity could be narrowed to the regions 276–308, which comprises exon 7 and

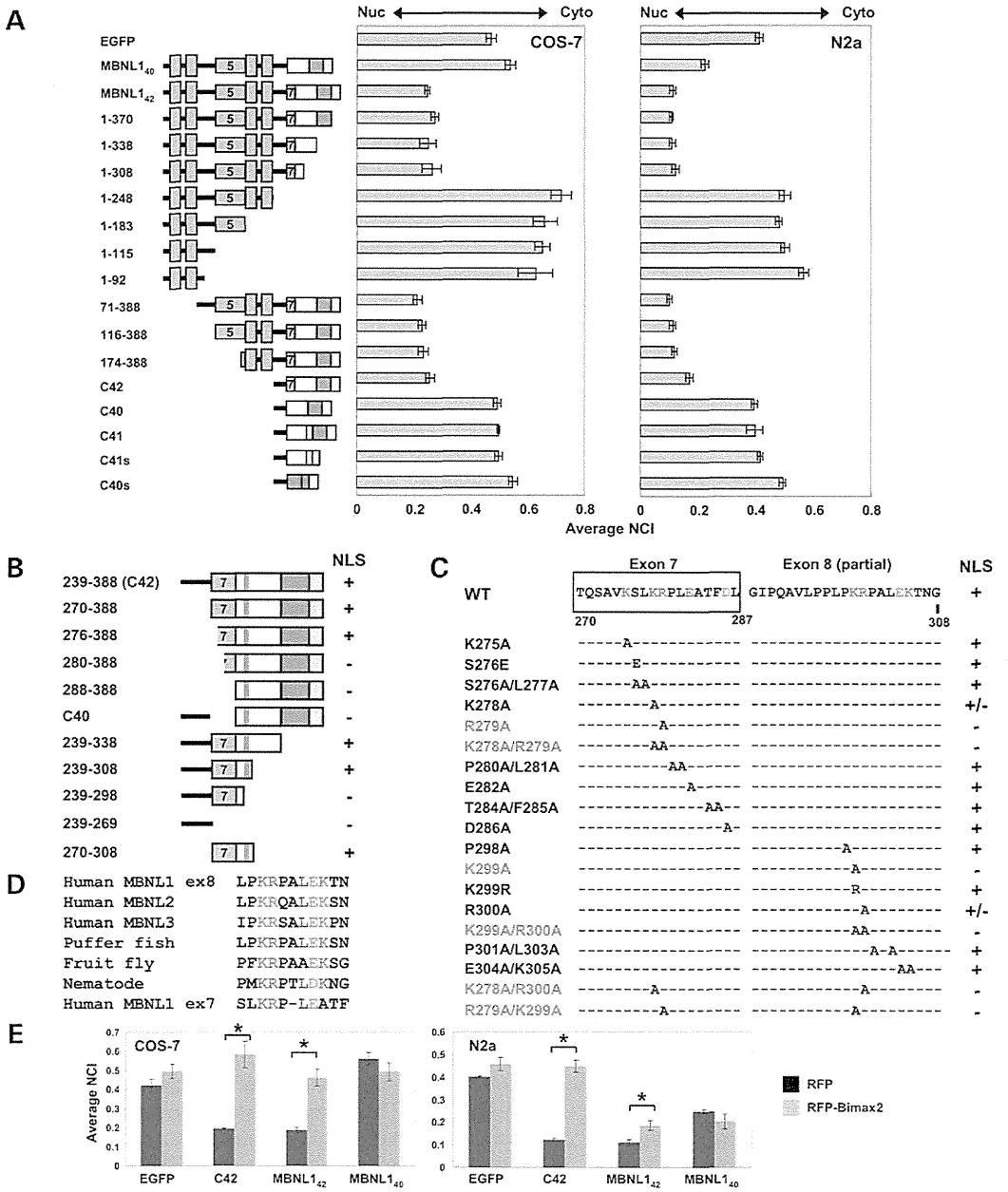

Figure 2. Determination of an NLS in the C-terminal region of $MBNL1_{42}$. (**A**) Intracellular localization of MBNL1 deletion mutants in COS-7 and N2a cells. Bar chart shows average NCI values of MBNL1 mutants (mean ± SD, $n = 3$). The structure of the transfected constructs is indicated at the left. (**B**) Nuclear localization of the C-terminal fragments of $MBNL1_{42}$ fused with EGFP. '+' indicates enhanced nuclear localization of the MBNL1 mutant. The results are based on the analysis of Supplementary Material, Figure S3A. (**C**) Point mutation analysis of $MBNL1_{42}$. Mutations were introduced into the full-length $MBNL1_{42}$ fused with EGFP. The results are based on the analysis of Supplementary Material, Figure S3B. (**D**) Evolutionarily conserved motif of exon 8. (**E**) The effect of RFP-fused Bimax2 peptide on the localization of MBNL1. Bar chart shows average NCI values in the presence and absence of RFP-Bimax2 (mean ± SD, $n = 3$). $^*P < 0.05$, two-tailed unpaired t-test ($n = 3$).

a part of exon 8 (Fig. 2B and Supplementary Material, Fig. S3A). Consistently, a peptide covering 270–308 was sufficient for driving nuclear localization (Fig. 2B and Supplementary Material, Fig. S3A). Point mutation analysis of this region in the context of full-length MBNL1$_{42}$ revealed the importance of four basic amino acids, K278, R279, K299 and R300 (Fig. 2C and Supplementary Material, Fig. S3B). Single point mutation of either R279A or K299A was sufficient for disrupting nuclear localization. In the case of K278A and R300A, single mutation showed little or no effect, whereas the simultaneous mutation of K278A and R300A completely disrupted nuclear localization (K278A/R300A, Fig. 2C and Supplementary Material, Fig. S3B). We also examined the effect of NLS mutations on the splicing activity. Both R279A and K299A mutants showed weakened splicing regulation of MBNL1, even though the protein expression of these mutants was equivalent to that of wild type (WT) (Supplementary Material, Fig. S3C and D).

All MBNL1 isoforms analyzed in this study, except for MBNL1$_{40s}$, contain a highly conserved motif in exon 8, KRPALE (Fig. 2D, Supplementary Material, Fig. S4A, and pink boxes in Fig. 2B). A corresponding motif in the fruit fly is involved in nuclear localization (30). However, this motif was not sufficient for mammalian MBNL1 nuclear localization, as demonstrated by the non-nuclear localization of C40 and 288–388, which contain this motif (Fig. 2B and Supplementary Material, Fig. S3A). The identified residues essential for nuclear localization were partly similar to a classical bipartite NLS (biNLS), which is typically summarized as KRX$_{(10\text{-}12)}$KR and acts through the importin α/β pathway. Co-expression of red fluorescent protein (RFP)-fused Bimax2 peptide, a specific inhibitor of the importin α/β pathway (38), prevented nuclear localization of C42 (Fig. 2E). Therefore, the NLS in the C-terminus of MBNL1 appears to be a bipartite NLS, even though the spacing of two KR motifs (19 amino acids) is larger than a typical biNLS (10–12 amino acids). In conclusion, both exon 7 and the conserved motif of exon 8 provide KR motifs that constitute a biNLS only when exon 7 is included in the alternative splicing.

The second NLS activity of MBNL1 involves multiple conserved motifs

During the above-mentioned analysis, we noticed a cell-type-dependent difference in nuclear localization of MBNL1. In N2a cells, MBNL1$_{40}$ showed significant nuclear localization despite the absence of exon 7 (Fig. 2A). Interestingly, Bimax2 disrupted nuclear localization of MBNL1$_{42}$ in COS-7 but only partially in N2a cells (Fig. 2E). Furthermore, nuclear localization of MBNL1$_{40}$ in N2a was not affected by Bimax2 (Fig. 2E). These results suggested that MBNL1 contains another NLS independent of the importin α/β pathway. We performed deletion analysis of MBNL1$_{40}$ (identical to 1-388Δex7 in Fig. 3A, a designation based on MBNL1$_{42}$ to maintain the amino acid numbering). In N2a cells, nuclear localization of MBNL1$_{40}$ required at least parts of both N- and C-terminus regions (Fig. 3A). Comparison of 1-308Δex7 and 1-298Δex7 demonstrated the necessity of the region around the conserved motif in exon 8 (pink box, Fig. 3A). In addition, deletion of an N-terminal region containing ZnF1/2 resulted in the loss of nuclear localization, as shown by 71-388Δex7 and 71-308Δex7 (Fig. 3A). Thus, the region around the conserved motif in exon 8 and the N-terminus region were essential for nuclear localization. We then tested point mutations of the conserved motif on exon 8 in the context of MBNL1$_{40}$. Similar to the case of MBNL1$_{42}$, mutation of K299A and R300A disrupted the nuclear localization of MBNL1$_{40}$ (Fig. 3B). However, other residues in the conserved motif were also essential for nuclear localization as revealed by the moderate to severe effects of P301D, A302D, L303A and E304A (Fig. 3B). This stood in contrast to the case of MBNL1$_{42}$, in which mutations of these residues did not affect nuclear localization (Fig. 2C).

Next, the involvement of the N-terminal region was examined. ZnF1/2 is a very highly conserved motif through evolution. We noticed that flanking regions of ZnF1/2 are also highly conserved and contain motifs, RD/KWL and KxQL/NGR (Fig. 3C and Supplementary Material, Fig. S4A). These motifs are not found in the flanking regions of ZnF3/4 of MBNL1 or other C3H ZnF proteins. Deletion of the first 13 amino acids from the N-terminus disrupted nuclear localization (Δ13, Fig. 3C). This could be partly explained by the depletion of the RD/KWL motif as shown by its mutation, mut(9-14) (Fig. 3C). Deletion of the KxQL/NGR motif, Δ(76-85), moderately weakened nuclear localization of MBNL1 (Fig. 3C). Interestingly, ZnF1/2, but not ZnF3/4, was found to contribute to nuclear localization (ΔZnF1/2 and ΔZnF3/4, Fig. 3C). Therefore, the N-terminal region of MBNL1 that comprises ZnF1/2 and its flanking motifs and the C-terminal conserved motif in exon 8 are essential for a second NLS activity of MBNL1. In contrast to the biNLS that comprises a linear motif, the second NLS was mediated by multiple and discrete regions of MBNL1. This is consistent with the recent classification of a conformational NLS (conNLS) (39).

We then analyzed whether the conNLS can act in the context of MBNL1$_{42}$ in N2a cells. A mutation of the KR motif in exon 7, which disrupts the biNLS, weakened but still preserved nuclear localization [1-388(K278A/R279A), Fig. 3D], suggesting that conNLS activity is present in MBNL1$_{42}$. However, deletion of a C-terminus region including the conserved motif of exon 8 also weakened but still preserved nuclear localization (Fig. 3D, compare 1–308, 1–298 and EGFP). This result was unexpected as this deletion was predicted to disrupt both biNLS and conNLS. Further deletion of exon 7 resulted in the loss of nuclear localization (1–269, Fig. 3D). Thus, exon 7 is involved in nuclear localization even in the absence of exon 8. As exon 7 itself was not sufficient for inducing nuclear localization (239–269, Fig. 2B), this effect of exon 7 requires the presence of the N-terminal region. We noticed that the sequence around the KR motif in exon 7 (KRPLE) is similar to that of the conserved motif in exon 8, KRPALE (Fig. 2D). When the KR motif of exon 7 was mutated in the context of 1–298, the mutant, 1–298 (K278A/R279A), exhibited loss of nuclear localization similar to 1–269 (Fig. 3D). Therefore, it appears that exon 7 contains another copy of the conserved motif and constitutes a conNLS together with the N-terminus region. In conclusion, MBNL1 has two classes of NLS (Fig. 3E). One is the biNLS consisting of two KR motifs embedded in conserved motifs of exons 7 and 8. The other is the conNLS, which involves the N-terminus region and either one of the conserved motifs in exon 7 or exon 8. Thus, MBNL1$_{42}$ possesses three possible NLS combinations, biNLS, conNLS using exon 7 and conNLS using exon 8. Most other isoforms contain only one conNLS using exon 8. MBNL1$_{40s}$ lacks any known NLS.

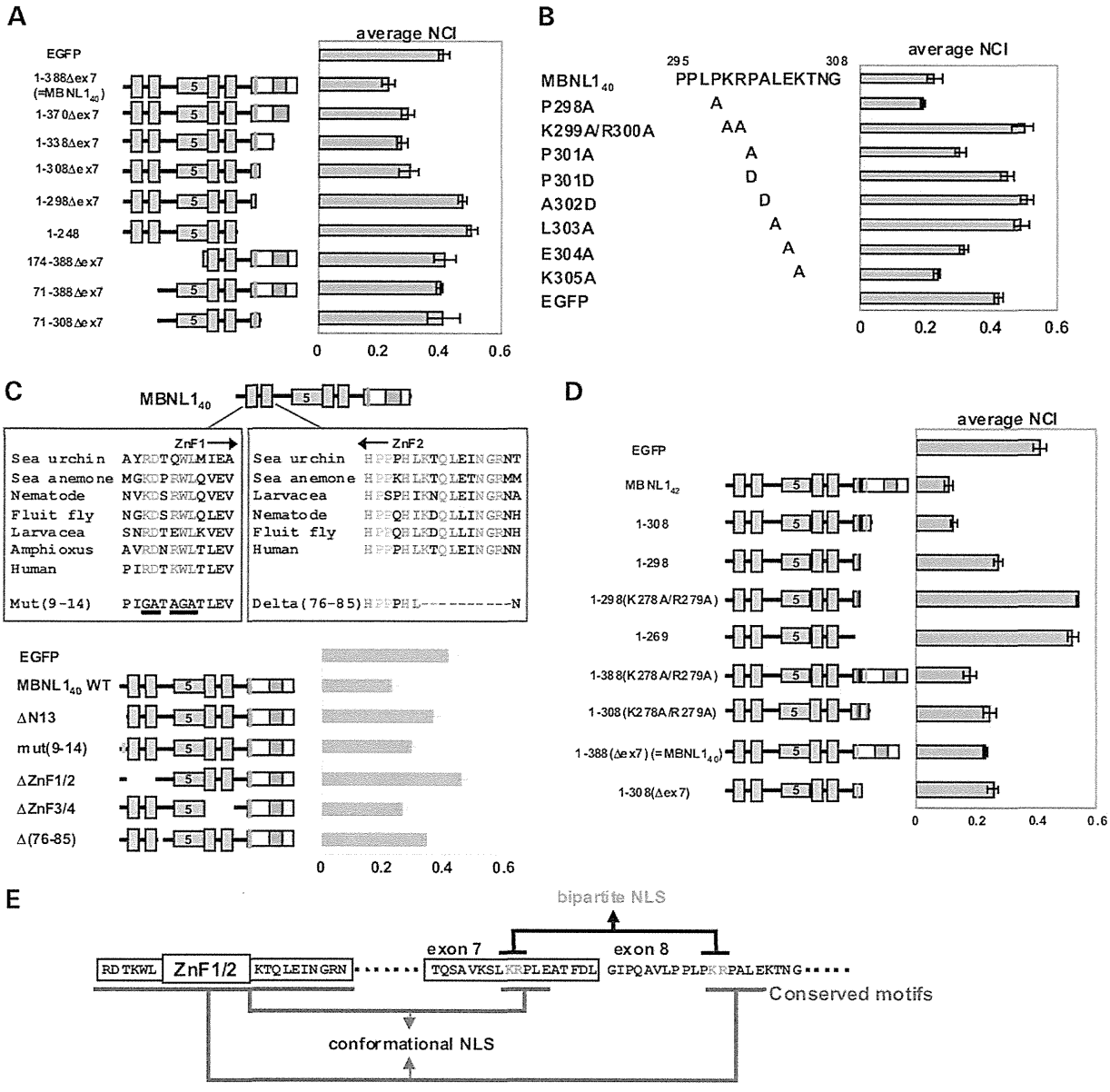

Figure 3. Identification of the second NLS activity of MBNL1. (**A**) Deletion analysis of MBNL1$_{40}$. Average NCI values of MBNL1$_{40}$ deletion mutants in N2a cells are indicated (mean ± SD, $n = 3$). 1-388Δex7 is identical to MBNL1$_{40}$. (**B**) The effects of point mutations on the localization of MBNL1$_{40}$. Mutations were introduced in the conserved motif of exon 8. Bar chart shows average NCI values as in (A). (**C**) Mutation analysis of conserved motifs in the N-terminus region of MBNL1. Evolutionary conservation of motifs flanking ZnF1/2 is shown at the top. Bar chart shows the nucleocytoplasmic localization of N-terminal mutants. The structure of the mutants is shown at the left. (**D**) The conserved motifs in exon 7 act as a part of a conNLS. Bar chart shows average NCI values as in (A). The structure of the mutants is shown at the left. (**E**) The mechanism of nuclear localization of MBNL1. See text for the detail.

Splicing-mediated coupling of MBNL activity and subcellular localization

As demonstrated earlier, exon 7 is an important determinant of the localization and function of MBNL1. In both N2a cells and adult mouse striatum, we detected Mbnl1 isoforms with and without exon 7 (Supplementary Material, Fig. S1A). Endogenous Mbnl1 was localized in the nucleus and cytoplasm (Supplementary Material, Fig. S5A). To analyze splicing regulation of this exon, we analyzed a minigene covering exons from 6 to 8 of mouse *Mbnl1*. Overexpression of the N-terminal regions of all three Mbnl paralogs strongly reduced the inclusion of exon 7 (Fig. 4A). In contrast to the case of *Actn1*, the N-terminus of Mbnl proteins did not require an NLS for strong repression of *Mbnl1* exon 7, suggesting the high sensitivity of this exon to Mbnl proteins. Co-expression of the *Mbnl1* minigene and a DMPK construct with an interrupted CTG480, but not CTG18, increased the inclusion of exon 7 (Fig. 4B). We also observed a small but significant increase in exon 7 inclusion when the

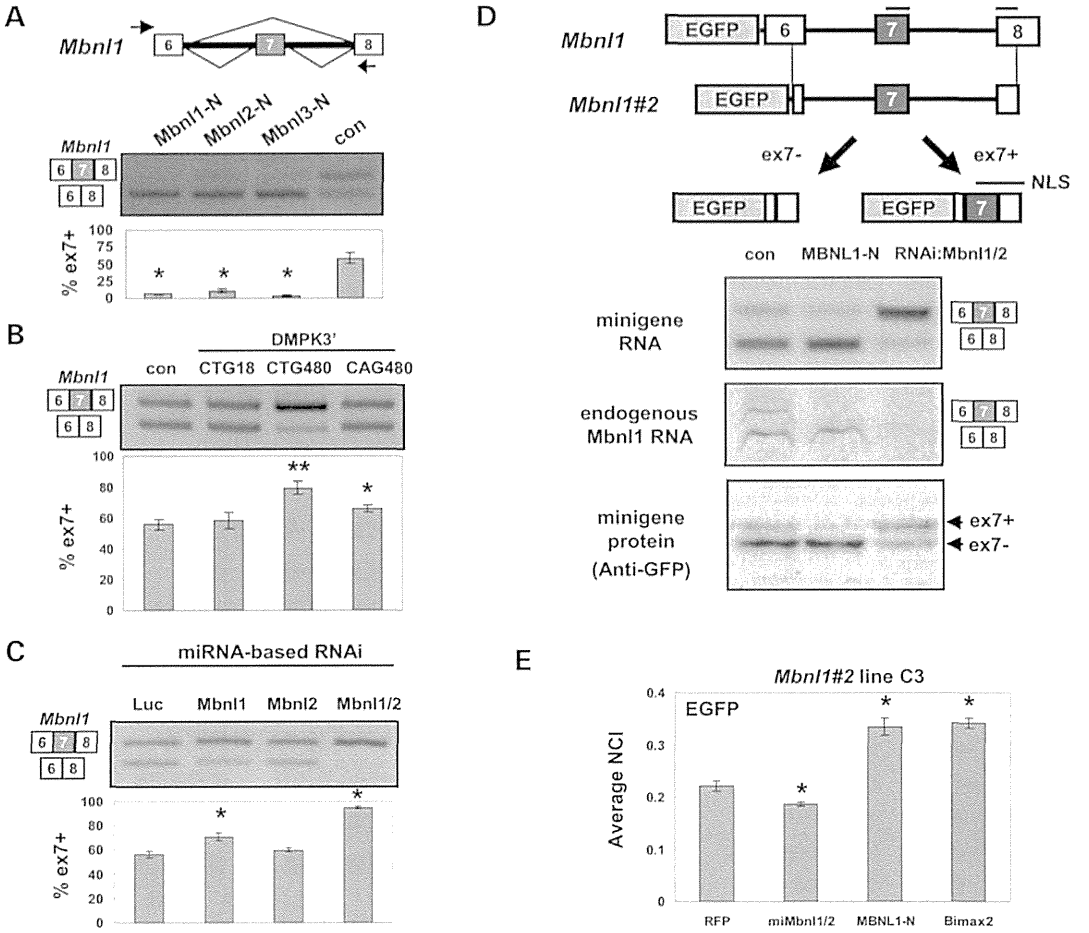

Figure 4. Splicing regulation of an *Mbnl1* minigene. (**A**) Structure of an *Mbnl1* minigene covering exons 6–8 (top). *Mbnl1* minigene is regulated by the N-terminus region of murine Mbnl paralogs in N2a cells (middle and bottom). Bar chart shows quantified results of the splicing assay (mean ± SD, $n = 3$). (**B**) Results of splicing assay using the *Mbnl1* minigene and DMPK3′ constructs with a normal or an expanded repeat. Results are shown as in (A). (**C**) The effect of RNAi-mediated depletion of endogenous Mbnl1 in N2a cells. Splicing assay of *Mbnl1* minigene was performed using cells depleted of Mbnl1 and/or Mbnl2 as indicated. Bar chart shows quantified results of the splicing assay (mean ± SD, $n = 3$). (**D**) An *Mbnl1* fluorescent minigene to examine the relationship between splicing pattern and localization. The *Mbnl1#2* minigene contains shortened exons 6 and 8. An N2a-based cell line stably expressing *Mbnl1#2* was established (line C3). Overexpression of MBNL1-N and simultaneous knockdown of endogenous Mbnl1 and Mbnl2 were examined. The splicing pattern of minigene mRNA (top) and endogenous Mbnl1 mRNA (middle) were detected by RT-PCR. Minigene protein was detected by western blot using anti-GFP antibody (bottom). (**E**) Quantified results of EGFP localization in the *Mbnl1#2* cell line C3 when MBNL1 was overexpressed or depleted. Overexpression of RFP-Bimax2 was also tested as a control of biNLS inhibition. Bar chart shows average NCI of RFP-positive cells (mean ± SD, $n = 3$). $^*P < 0.05$, Tukey's test for multiple comparison ($n = 3$).

CAG480 construct was overexpressed (Fig. 4B). RNAi-mediated knockdown of endogenous Mbnl1 induced a moderate increase in the inclusion of exon 7, whereas knockdown of Mbnl2 alone exhibited little effect (Fig. 4C and Supplementary Material, Fig. S2D). Importantly, simultaneous knockdown of both Mbnl1 and Mbnl2 increased exon 7 inclusion more strongly than that of Mbnl1 alone (miMbnl1/2, Fig. 4C and Supplementary Material, Fig. S2D). These results demonstrated that alternative splicing of *Mbnl1* exon 7 is regulated by MBNL proteins in a dose-dependent manner. We confirmed intracellular association between EGFP-MBNL1 and endogenous *Mbnl1* transcripts by ribonucleoprotein immunoprecipitation analysis using a cell line stably expressing EGFP-MBNL1$_{40}$ (Supplementary Material, Fig. S4B). Thus, MBNL1 associates with its transcript and autoregulates alternative splicing.

As the *Mbnl1* minigene contains a region corresponding to the biNLS identified earlier, we expected that the localization of EGFP fused upstream of the minigene might be changed according to the splicing pattern of exon 7. However, the EGFP fluorescence of this construct was not strong enough to be detected clearly. We made another shortened minigene (Mbnl1#2, Fig. 4D), which still contained the biNLS region and showed stronger fluorescence than the original minigene. A N2a-based cell line stably expressing this minigene showed EGFP fluorescence in both nucleus and cytoplasm (Supplementary Material, Fig. S4C). Patterns of minigene-derived protein or RNA were altered when MBNL1 was overexpressed or knocked down (Fig. 4D). The patterns of the transcript and the protein expressed from the minigene were altered depending on the dose of MBNL1 (Fig. 4D). Notably, cytoplasmic localization of EGFP

was enhanced when MBNL1 was transfected, whereas nuclear localization was enhanced when endogenous Mbnl1 and Mbnl2 were knocked down (Fig. 4E and Supplementary Material, Fig. S4C). Thus, alternative splicing of *Mbnl1* exon 7 directly reflects the activity of MBNL proteins and alters nucleocytoplasmic localization of MBNL1. This mechanism can be regarded as a dynamic negative feedback where an increase in nuclear MBNL activity leads to a decrease in the production of nuclear isoform containing exon 7.

MBNL1 promotes nuclear accumulation of RNA with expanded CUG and CAG repeats

Next, we analyzed the effect of MBNL1 on the localization of transcripts containing expanded CUG or CAG repeats. It has been known that CUG repeat-containing RNA is retained in the nucleus and co-aggregates with MBNL1 (10). As reported previously (32), knockdown of MBNL proteins greatly reduced RNA foci in DM1 fibroblasts (Supplementary Material, Fig. S11B and C), indicating an essential role of MBNL proteins in RNA foci formation. We then used constructs that contain an interrupted repeat similar to the ones widely used in DM1 studies (Supplementary Material, Fig. S6A). CUG-repeat RNA in the context of a DMPK fragment (DMPK3′-CTG480) was visualized by fluorescence in situ hybridization (FISH). Unexpectedly, many cells showed RNA localization in the cytoplasm (Fig. 5A). In contrast, co-transfection of $MBNL1_{42}$ with the repeat constructs greatly enhanced nuclear accumulation of repeat RNA mainly as foci (arrows, Fig. 5B and Supplementary Material, Fig. S7A and B). We quantified the relative nucleocytoplasmic distribution of repeat RNA based on the FISH signal. Nuclear localization of CUG repeat was enhanced by $MBNL1_{42}$ compared with EGFP (Fig. 5C). Mutation analysis revealed that the enhancement of nuclear RNA localization was dependent on the composition of zinc finger motifs (comparison of MBNL1-N versus 71–248), linker region ($MBNL1_{40}$ versus $MBNL1_{35}$ and 71–388 versus 174–388) and nuclear localization (NLS-MBNL1-N versus NES-MBNL1-N) (Fig. 5C and Supplementary Material, Fig. S8A, and see also Fig. 2A for the localization of MBNL1 mutants). We also tested non-coding repeats in a DMPK-independent context, in which CTG or CAG repeat is downstream of a CMV promoter and no ATG codon is located between the promoter and the repeat. As with DMPK3′-CTG480, CAG240 did not show an efficient nuclear accumulation in the absence of $MBNL1_{42}$ overexpression (Fig. 5D). Thus, expanded RNA alone does not efficiently accumulate in the nucleus in the absence of a sufficient amount of MBNL1. Comparative analysis of CAG and CTG constructs with various lengths (Supplementary Material, Fig. S8B) revealed that (i) CUG-repeat RNA tends to show stronger nuclear localization than the length-matched CAG repeat, (ii) $MBNL1_{42}$ enhanced nuclear localization of both CAG and CUG repeats, whereas MBNL1-N showed weak effects on CAG repeats and (iii) even the same size of repeat (CTG480) can have differential degree of nuclear localization depending on the context (V5 versus DMPK′3). We also analyzed mutual effects of repeat RNA and MBNL1 on their nucleocytoplasmic localization. We used MBNL1 variants with partial cytoplasmic localization, $MBNL1_{40}$ (containing a conNLS) and MBNL1-N (containing no NLS). While these proteins enhanced nuclear localization of RNA, that of these proteins were not altered (Fig. 5E). Finally, knockdown of Mbnl proteins increased cytoplasmic localization of CUG repeat (Fig. 5F). These results suggest that the nuclear retention of CUG-repeat RNA can be actively caused by MBNL1 in the nucleus. Interestingly, we noticed that most endogenous Mbnl1 was located outside of RNA foci that were induced by MBNL overexpression (Supplementary Material, Fig. S7C). We also examined a CAA repeat as a control. Although CAA108 occasionally formed nuclear foci, EGFP-$MBNL1_{42}$ did not colocalize with them (Supplementary Material, Fig. S9A). Moreover, both overexpression and knockdown of MBNL1 did not affect the localization of CAA-repeat RNA (Supplementary Material, Fig. S9B and C). Thus, the effect of MBNL1 is dependent on repeat sequences.

MBNL1 suppresses the expression of aberrant proteins containing an expanded CUG or CAG repeat

A recent study reports protein expression from expanded repeats in the absence of an initiation codon, in which the repeats tract could be translated in all three frames (21). We examined whether any proteins are expressed from the non-coding repeat constructs used in Figure 5D (CTG240 and CAG240). CAG240 produced a high-molecular-weight protein detected by antibody against V5-tag, which is located downstream of the repeat tract (Fig. 6A). We also examined different lengths of CAG and CTG repeats. Interestingly, CAG constructs expressed V5-positive proteins in a length-dependent manner with peak expression at 360 repeats. In contrast, CTG constructs did not express proteins detected by anti-V5 (Fig. 6A). Owing to 5-base interruptions for every 20 CAG or CTG repeats, the interrupted CAG and CTG repeat tracts encode $(Q20\text{-}S22\text{-}A20)_n$ and $(C20\text{-}A20\text{-}L21)_n$ polypeptides, respectively, if translated (Supplementary Material, Fig. S6A). The large protein expressed from the CAG construct was detected by 1C2 antibody, indicating the presence of polyQ tracts. In the absence of an apparent start codon upstream of the repeat tract, the reading frame of the repeat is not clear. We examined three different reading frames of the V5 tag downstream of the repeat tract (Fig. 6B); reading frame 1 was used in the above-mentioned experiments. CAG-repeat constructs with different reading frames produced high-molecular-weight proteins detected by anti-V5 and 1C2 antibodies (Fig. 6B). These constructs showed some difference in the pattern of lower-molecular-weight proteins (corresponding to 40–70 kDa) (Fig. 6B). In contrast, little or no protein was expressed from the CTG constructs with different reading frames of the V5 tag (Fig. 6B). Next, we tested the effect of MBNL1 on the expression of the protein from the CAG construct. When the CAG360 construct was co-expressed with $MBNL1_{42}$ or $MBNL2_{42}$, the anti-V5-reactive product was decreased compared with control (Fig. 6C). $MBNL1_{42}$ enhanced nuclear localization of CAG360 mRNA (Supplementary Material, Fig. S8B). Simultaneous knockdown of both Mbnl1 and Mbnl2 increased the expression of CAG360 (Fig. 6D). Therefore, nuclear retention of repeat-containing RNA induced by MBNL1 can result in the reduction of aberrant proteins expressed from the repeat RNA.

MBNL1 suppresses the expression of polyglutamine-containing proteins

As shown earlier, MBNL1 can alter the localization of seemingly non-coding CAG repeats and reduce the expression of

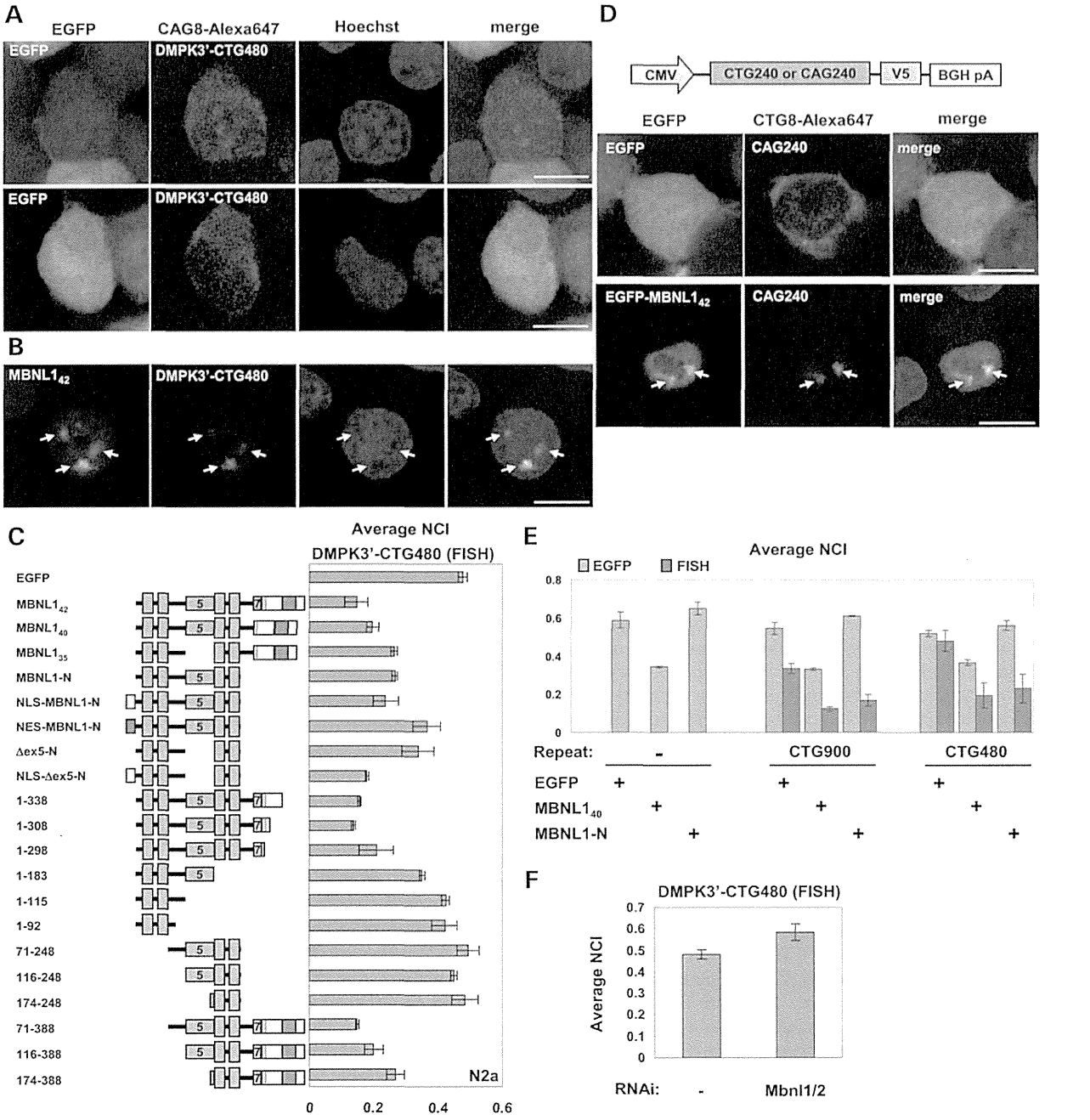

Figure 5. MBNL1 induces nuclear retention of repeat RNA. (**A** and **B**) Intracellular localization of CUG repeat in the context of the 3′ region of DMPK 3′. DMPK3′-CTG480 was transfected with either EGFP (A) or EGFP-MBNL1$_{42}$ (B) in N2a cells, and the localization of repeat RNA was detected by FISH. (**C**) Quantitative analysis of CUG-repeat RNA detected by FISH. DMPK3′-CTG480 was transfected with EGFP or EGFP-MBNL1 mutants as indicated. Bars indicate average NCI (mean ± SD, $n = 3$). See also Supplementary Material, Figure S8A. (**D**) Structure of non-coding repeat construct (top). Long interrupted CTG or CAG repeat was inserted between CMV promoter and a V5 tag. Intracellular localization of CAG240 RNA co-transfected with EGFP (middle) or EGFP-MBNL1$_{42}$ (bottom). Nuclear staining with Hoechst33342 is included in the merged panels. (**E**) Quantitative analysis of nucleocytoplasmic localization of MBNL1 variants and repeat RNA in N2a cells co-expressing them. For RNA expression, repeat tracts in the DMPK3′ context were transfected with EGFP or EGFP-fused MBNL1 variants. Intracellular localization of EGFP and FISH signals in GFP/Alexa-546 double-positive cells was quantified (mean ± SD, $n = 3$). As a control, the localization of proteins was quantified in the absence of RNA constructs. (**F**) The effect of depletion of endogenous Mbnl1/2 on the RNA localization of DMPK3′-CTG480. Bar chart shows RNA localization as in (C). In (B and D), arrows indicate RNA foci. Scale bar indicates 10 μm.

polyQ-containing proteins. We next asked whether MBNL1 can alter the expression from apparently coding CAG repeats. For this purpose, the effect of MBNL1 on the localization of huntingtin exon 1 RNA was tested. Similar to the results in Figure 5, MBNL1 enhanced the nuclear localization of CAG-containing mRNA of huntingtin, as seen by FISH analysis

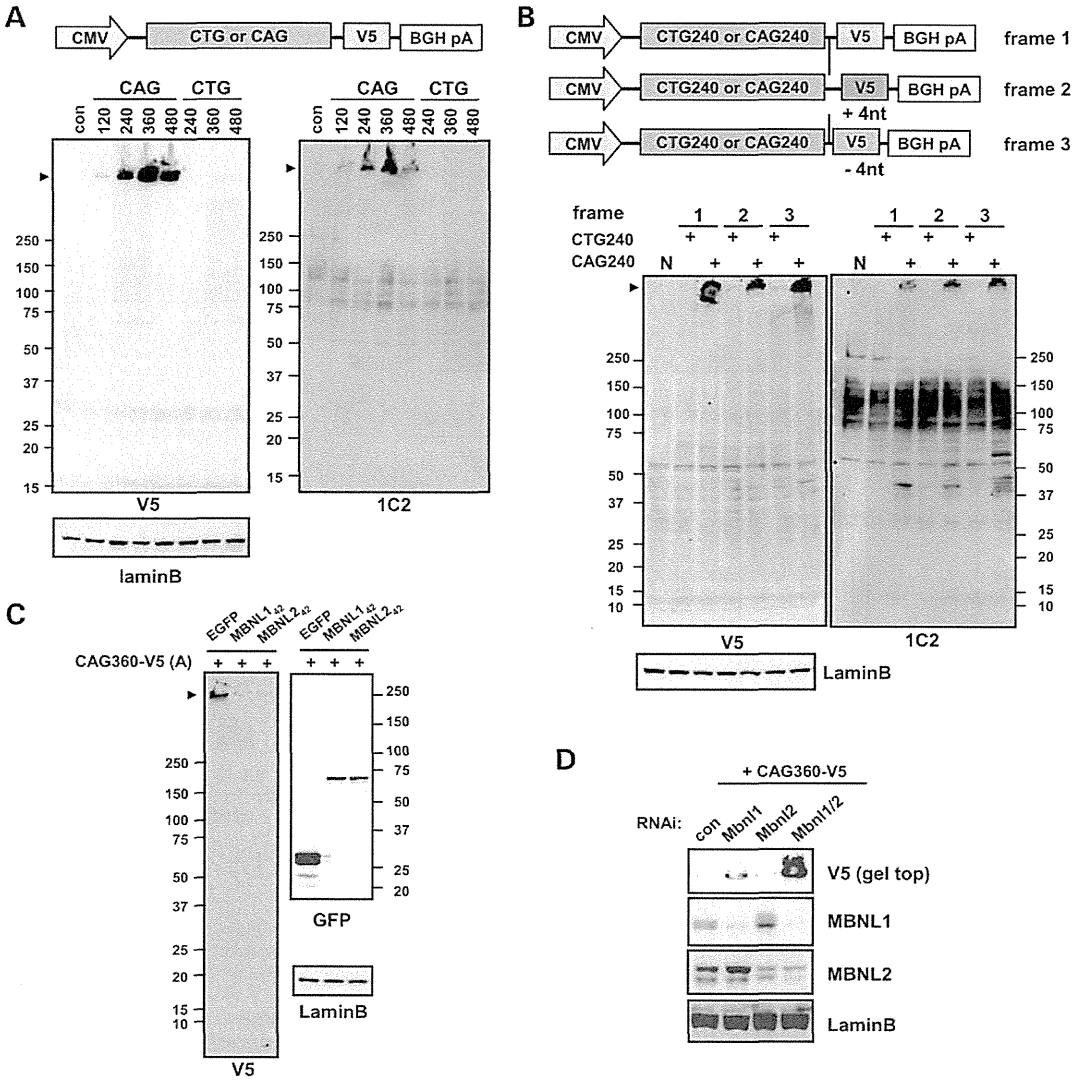

Figure 6. MBNL1 induces nuclear retention of repeat RNA. (**A**) Structure of non-coding repeat constructs. A long, interrupted CTG or CAG repeat was inserted between the CMV promoter and a V5 tag. There is no ATG codon located between the CMV promoter and the repeat tract. (**B**) Three different reading frames of V5 tag relative to the repeat tract were prepared. Repeat-derived proteins expressed from the CAG or CTG constructs. Protein expression was detected using anti-V5 and 1C2 antibodies. Lamin B served as a loading control. (**C**) Western analysis of the expression of CAG-repeat-derived proteins co-transfected with EGFP, EGFP-MBNL1$_{42}$ or EGFP-MBNL2$_{42}$. (**D**) Western analysis of the aberrant protein from the CAG360 construct with or without RNAi treatment for Mbnl1 and/or Mbnl2.

(Fig. 7A and B). When protein expression was examined, co-expression of EGFP-MBNL1 greatly reduced mutant huntingtin protein fused with RFP or V5 tag detected mainly at the gel top (Fig. 7C and Supplementary Material, Fig. S6B). Reduction in protein expression was much milder for huntingtin with CAG18 (Fig. 7C). Knockdown of both Mbnl1 and Mbnl2 resulted in the accumulation of mutant huntingtin (Fig. 7D). Depletion of Mbnl1/2 also led to cytoplasmic localization of mutant huntingtin mRNA and increased the cytotoxicity (Fig. 7E and F). RNAi-resistant mutant of MBNL1$_{42}$, MBNL1(res)$_{42}$, but not WT MBNL1$_{42}$ counteracted the effect of Mbnl1/2 knockdown (Supplementary Material, Fig. S10). The expression of RFP-fused CAG78 encoding Q78 was reduced by the expression of MBNL1 (Supplementary Material, Fig. S6C). Furthermore, MBNL1 reduced the expression of EGFP-fused CAG78 in different reading frames, which expressed polyglutamine, polyalanine or polyserine (Supplementary Material, Fig. S6D). Thus, the repressive effect of MBNL1 was independent of the context of huntingtin and was not restricted to the reading frame of polyQ. In conclusion, MBNL1 has a repressive effect on the expression of CAG-repeat-derived proteins.

In primary cultured mouse cortical neurons, we observed RNA foci and RNA localization in the nucleus and cytoplasm when DMPK3′-CTG480 or mutant huntingtin exon 1 was transfected with EGFP, whereas co-expression of MBNL1$_{42}$ enhanced the localization of repeat RNA in the nuclear foci (Fig. 8A and Supplementary Material, Fig. S11A). We also analyzed the striatum of HD model mice, the R6/2 strain. Transcripts

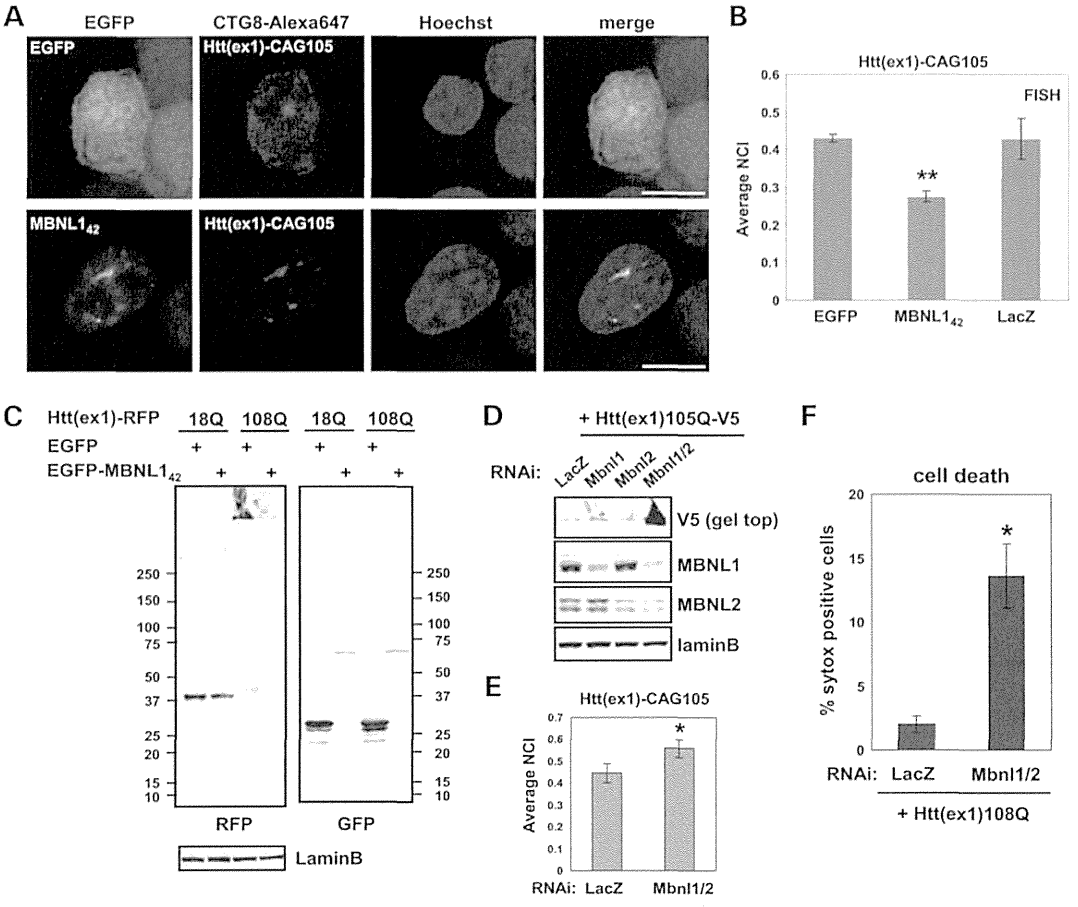

Figure 7. MBNL1 represses the expression of expanded huntingtin exon 1. (**A**) Nucleocytoplasmic localization of huntingtin exon 1 mRNA was altered by EGFP-MBNL1$_{42}$. The huntingtin construct contains CAG105 and a V5 tag sequence. The localization of huntingtin mRNA was detected by FISH using Alexa-647-labeled CTG8 oligonucleotide. Scale bar indicates 10 μm. (**B**) Quantitative localization analysis of (A). Bar chart indicates average NCI of the CAG-repeat RNA of huntingtin detected by FISH (mean ± SD, $n = 3$). $^{**}P < 0.005$ in comparison with EGFP (Tukey's multiple test). (**C**) Western analysis of the effect of EGFP-MBNL1 on the expression of RFP-fused huntingtin exon 1 with CAG18 or CAG108 in N2a cells. Transfected proteins were detected using anti-GFP and anti-RFP. (**D**) Western analysis of the effect of RNAi-mediated knockdown of MBNL1 and/or MBNL2 on the expression of huntingtin exon 1 with CAG105 in N2a cells. Huntingtin was detected by anti-V5 antibody. Knockdown of endogenous Mbnl1 and Mbnl2 was confirmed by specific antibodies. Lamin B serves as a loading control. (**E**) Huntingtin mRNA localization was altered by RNAi-mediated knockdown of Mbnl1 and Mbnl2 ($^{*}P < 0.05$, two-tailed t-test; $n = 3$). (**F**) The effect of depletion of Mbnl proteins on the cytotoxicity of mutant huntingtin. RNAi vectors expressing RFP were transfected with mutant huntingtin and treated with sytox green to label dying and dead cells. The fraction of cells with both green and red signals in the total transfected cells (red positive cells) were quantified (mean ± SD). $^{*}P = 0.022$ (two-tailed unpaired t-test, $n = 6$). RNAi treatment of Mbnl1/2 itself did not show cytotoxicity (data not shown).

from Huntingtin transgene were detected by FISH in the transgenic (TG) mice but not in the WT control (Fig. 8B). Mutant RNA were localized mostly in the cytoplasm, and we hardly observed RNA foci in the nucleus (Fig. 8B). Mbnl proteins were distributed in both nucleus and cytoplasm, and the staining patterns were similar between WT and TG mice, except for slight reduction of Mbnl2 staining in TG mice reflecting reduction in its mRNA level (Fig. 8C, Supplementary Material, Fig. S2G). Alternative splicing of Mbnl1 exon 7 was not altered in TG mice (Fig. 8D), suggesting that the function of Mbnl proteins was preserved in TG mice. In cells derived from striatal neurons of HD knock-in mice (StHdh 111/111), we did not detect specific FISH signals above background, as we observed diffuse staining in StHdh 7/7 that may reflect CAG-containing transcripts other than huntingtin (Fig. 8E, upper panels). However, overexpression of MBNL1$_{42}$ manifested RNA foci in StHdh 111/111 cells (Fig. 8E, lower panels). These results suggest that the expression of expanded-repeat transcripts is not sufficient for RNA foci formation in some cell-types. However, overexpression of MBNL proteins could induce RNA foci formation and/or nuclear RNA retention in such cells.

DISCUSSION

Interplay of conserved motifs determines nuclear localization of MBNL1

Though previous studies indicated that exon 7 of MBNL1 is involved in nuclear localization (11,31,40), the mechanism has been uncharacterized. Here, we clarified the role of exon 7 in nuclear localization. Two clusters of KR residues in the C-terminus region were essential for the function of the NLS.

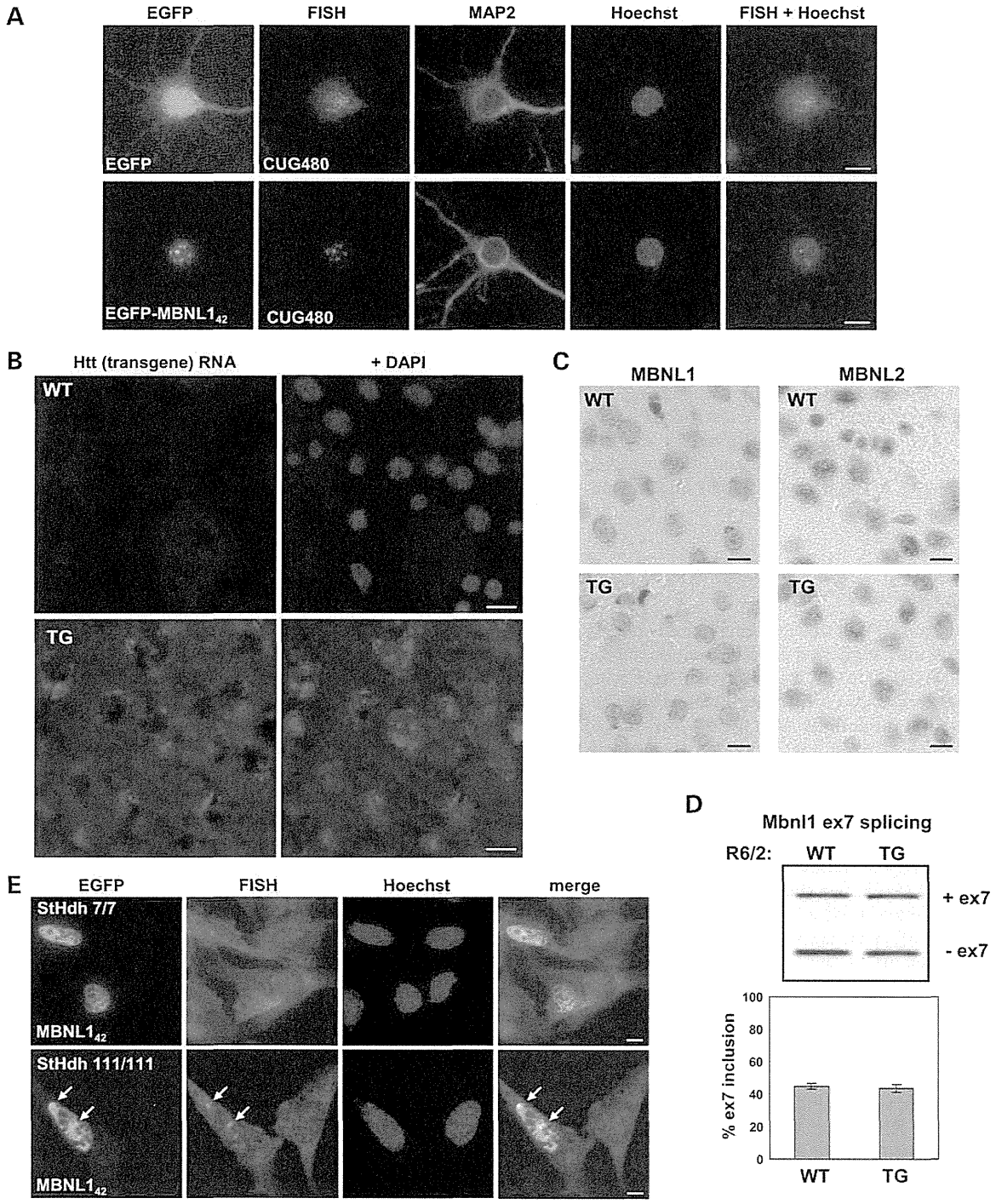

Figure 8. Localization of expanded RNA and MBNL proteins in cultured neurons and disease model cells. (**A**) Subcellular localization of mRNA of DMPK3′-CTG480 in primary cultured cortical neurons. The localization of repeat RNA was detected by FISH using Cy3-labeled CAG8. MAP2 serves as a marker of neurons. (**B**) FISH analysis of huntingtin transgene in the striatum of R6/2 mice. Mutant huntingtin mRNA was detected using DIG-labeled antisense RNA of human huntingtin. (**C**) Immunohistochemical analysis of Mbnl proteins in the striatum of R6/2 mice. (**D**) Splicing analysis of *Mbnl1* exon 7 in the striatum of R6/2 mice. The inclusion of exon 7 was not different between WT and TG mice ($n = 4$). (**E**) FISH analysis of StHdh cells transfected with EGFP-MBNL1$_{42}$. RNA foci were detected in StHdh 111/111 cells expressing EGFP-MBNL1 (arrows), but not in untransfected cells. Scale bars indicate 10 μm.

The activity of this NLS was inhibited by a specific inhibitor of the importin alpha/beta pathway (Bimax2), clearly demonstrating that the two KR clusters constitute a biNLS. We also found the second NLS that is dependent on the cell type. This latter NLS involves multiple conserved regions of the protein (Fig. 3E). None of the conserved motifs, namely KRPALE, ZnF1/2, RD/KWL and KxQL/NGR, was sufficient for the NLS activity by itself. Thus, the second NLS is consistent with a conNLS (39). It is currently unclear which import pathway mediates the activity of the conNLS. As ZnF1/2 is involved in RNA-binding activity (9), the status of RNA binding of MBNL1 might be related to the activity of the conNLS. We also found that MBNL1 contains two KRP(A)LE motifs in exons 7 and 8 and that each of these motifs can act as a part of the conNLS. Thus, $MBNL1_{42}$ can utilize two combinations of the conNLS in addition to the biNLS. Therefore, the inclusion of exon 7 acts as a switch for multiplying the pathways of nuclear import, ensuring efficient nuclear localization. Finally, the residues in the KRP(A)LE motifs are differently required in the context of biNLS and conNLS (Figs 2C and 3B), providing a unique example of motif usage in two different import pathways.

Alternative splicing of exon 7 couples nuclear activity and intracellular localization of MBNL1

It has been suggested that MBNL1 autoregulates exon 7 splicing (11,29). Mouse studies also suggested cross-regulation among MBNL proteins (11,41). Here, we show that alternative splicing of exon 7 directly couples activity of MBNL proteins and nuclear localization of MBNL1 at the cellular level. Overexpression of any Mbnl paralogs repressed exon 7 inclusion, whereas simultaneous knockdown of Mbnl1 and Mbnl2 was required for efficient skipping of exon 7 (Fig. 4A and C). MBNL2 has an alternative exon corresponding to exon 7 of MBNL1, which is involved in the nuclear localization as well as splicing activity of MBNL2 (Supplementary Material, Fig. S2B and C) and is misregulated in DM1 (11). These explain why knockdown of either Mbnl1 or Mbnl2 showed weak effects on the splicing regulation and the repression of repeat-derived proteins (Figs 4C, 6D and 7D), because a reduction in one MBNL protein would be compensated by the increased nuclear isoforms of the other MBNL protein. Importantly, we showed that the NLS activity of MBNL1 closely reflects its splicing activity in a dynamic manner using a cell line expressing a fluorescent minigene, demonstrating that depletion of Mbnl proteins induced nuclear accumulation of the *Mbnl1* minigene (Fig. 4D and E). Moreover, co-expression of repeat RNA and MBNL1 *per se* did not induce translocation of cytoplasmic MBNL1 into the nucleus (Fig. 5E), suggesting that an extensive nuclear accumulation of MBNL1 observed in disease conditions may require enhanced production of nuclear isoforms. Altogether, we established an activity-dependent nuclear localization of MBNL1, in which MBNL isoforms containing exon 7 are predominantly produced when the nuclear amount or activity of MBNL proteins is low, whereas isoforms without exon 7 are predominantly produced after the amount of nuclear MBNL proteins reaches a certain amount. This mechanism would keep the amount of nuclear MBNL protein to a certain level in an autoregulatory feedback loop (Fig. 9A) and suggests the status of exon 7 splicing as an indicator of MBNL activity. Moreover, the increase of nuclear isoforms in disease conditions would accelerate the interaction between MBNL1 and CUG-repeat RNA in the nucleus (Fig. 9B).

Repression of aberrant protein expression by MBNL1

Previous reports suggest that knockdown of MBNL proteins reduces RNA foci formation (32–34). We have shown that MBNL1 promotes the accumulation of expanded-repeat-containing RNA in the nucleus. As a consequence of nuclear RNA retention, MBNL1 represses the expression of mutant protein from transcripts containing an expanded CAG repeat (Figs 6 and 7). The effect of MBNL1 was observed for both coding and non-coding repeat tracts. To date, mislocalization or accumulation of MBNL1 in the nuclear foci has been thought to cause a loss of MBNL1 function leading to misregulation of alternative splicing (Fig. 9B). We propose that such accumulation of MBNL1 has another aspect, the repression of cytoplasmic transport of mutant RNA and its subsequent translation (Fig. 9B). This process might be regarded as an RNA quality control mechanism that limits the production of aberrant proteins from non-physiological transcripts with certain structural properties. Thus, MBNL1 is not simply a victim of expanded repeats but can be a guardian against protein toxicity. As MBNL proteins have cytoplasmic roles (42,43), we do not rule out the contribution of cytoplasmic MBNL1 in repressing repeat-derived proteins.

We observed protein expression from non-coding repeats with interruptions, which have not been examined previously (21). We observed the expression of polyQ-containing proteins from interrupted CAG repeats, which were repressed by MBNL proteins (Fig. 6C). Importantly, similar results were obtained for mutant huntingtin with a pure CAG repeat (Fig. 7C), suggesting that some important properties of pure repeats are retained in interrupted repeats. We hardly observed protein expression from interrupted CTG repeats even when Mbnl proteins were depleted (data not shown). There might be an orientation-dependent preference in the expression of these repeats. Consistently, RAN translation is dependent on the context surrounding the repeat (21). Alternatively, the homopolymeric proteins may have different susceptibility to degradation.

RNA-binding proteins as potential modifiers of repeat expansion diseases

Our results suggest MBNL proteins as potential modifiers of polyQ diseases. Interestingly, MBNL1-containing RNA foci were recently detected in the fibroblasts of human HD and spinocerebellar ataxia type 3 (24,44). However, RNA foci were hardly detected in HD model mice and cells derived from HD knock-in mice, in our hands. There might be cell-type-dependent differences in the interaction between MBNL proteins and repeat RNA. Mbnl2 is a major MBNL protein in the mouse brain (Supplementary Material, Fig. S2F). We observed a slight reduction in the expression of Mbnl2 (Fig. 8C and Supplementary Material, Fig. S2G). However, alternative splicing of *Mbnl1* exon 7 was unchanged, suggesting that the activity of Mbnl proteins was not markedly altered in HD mice. In contrast, MBNL proteins are found in RNA foci in DM1 and SCA8 that is accompanied by splicing misregulation of *Mbnl1* exon 7 (8,11,28). These

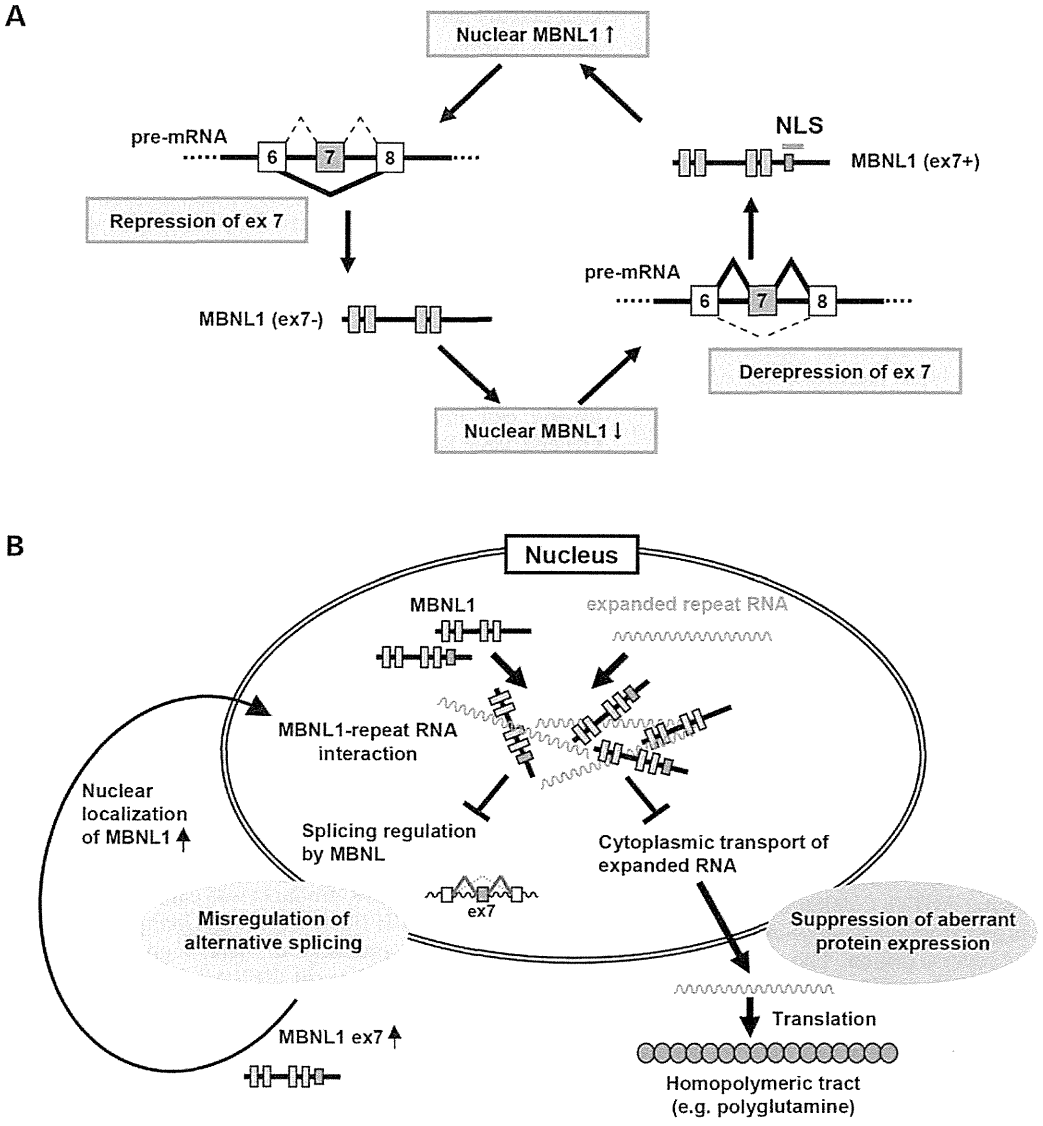

Figure 9. Autoregulation of MBNL1 and a novel aspect of MBNL–RNA interaction in the nucleus. (**A**) Autoregulation of MBNL1. Nuclear MBNL function can be maintained through feedback autoregulation. Increased activity of MBNL proteins in the nucleus leads to exon 7 skipping, which results in the production of MBNL1 isoforms lacking an NLS. This may in turn lead to reduced MBNL activity in the nucleus, resulting in an increase in exon 7 inclusion. Such a feedback mechanism may limit the amount of nuclear MBNL proteins. (**B**) In the presence of expanded-repeat RNA as in disease conditions, the activity of MBNL proteins is reduced, leading to enhanced exon 7 inclusion. This in turn leads to accumulation of MBNL1-containing NLS in the nucleus and may enhance interaction with expanded-repeat RNA. The interaction of MBNL1 and repeat RNA also causes nuclear retention of the repeat RNA, which prevents the expression of aberrant homopolymeric proteins such as polyQ.

results are consistent with the notion that repeat-MBNL interaction induces RNA foci formation that have two consequences, reduced MBNL activities and suppression of repeat-derived proteins (Fig. 9B). In HD mice and StHdh cells, this interaction was somehow inefficient, possibly because (i) expanded CAG repeat binds to MBNL proteins less strongly than CUG repeat, (ii) the length of CAG repeat was relatively short, (iii) the level of endogenous MBNL proteins or mutant RNA was not sufficient and/or (iv) some co-factor or modifications of Mbnl proteins were lacked in the brain of HD mice and/or StHdh cells. However, in all cell types we have tested, overexpression of $MBNL1_{42}$ induced RNA foci formation, suggesting that a certain level of nuclear MBNL proteins can overcome the limitations mentioned earlier. Our results would warrant further investigations of HD mouse models based on the overexpression of MBNL proteins.

MBNL proteins might provide a basis for the development of therapies to reduce aberrant protein expression associated with repeat expansion. For example, compounds that mimic MBNL1 and induce nuclear retention of mutant transcripts would prevent toxic effects of homopolymeric proteins (45). Another therapeutic implication is that MBNL-mediated

nuclear RNA retention would facilitate selective degradation of mutant RNA, as RNA in the nucleus is susceptible to antisense oligonucleotide-mediated degradation (46).

Recently, dipeptide repeat proteins were found in C9-ALS/FTD that is caused by a hexanucleotide repeat expansion (47–52). In addition, polyglycine-containing protein was found in fragile X-associated tremor/ataxia syndrome (FXTAS) (50). These repetitive proteins are generated from non-coding tracts through RAN translation. The pronounced expression of expanded-repeat-derived proteins in HD, C9-ALS/FTD and FXTAS indicates that nuclear retention of expanded RNA might be inefficient in the cells of these diseases. Remarkably, the distributions of RNA foci and dipeptide repeat inclusions were largely segregated in the brain regions of C9-ALS/FTD (52), consistent with our model of reciprocal relationship between RNA foci formation and RAN translation (Fig. 9B) and its dependence on cell types. Owing to RAN translation, all transcribed repeat tracts may potentially have both RNA and protein toxicities (21). The relative contribution of these toxicities in each disease would be an important future subject. Our results suggest the importance of RNA-binding proteins as key factors involved in both RNA- and protein-mediated pathogenesis of repeat expansion diseases.

MATERIALS AND METHODS

cDNA clones and constructs

cDNA of human MBNL1, MBNL2 and MBNL3 were described previously (37). To facilitate mutagenesis, a silent mutation of L281L (c843t), which eliminates a XhoI site, was introduced into MBNL1 cDNA and the mutant was designated MBNL1/L281L. For making MBNL1 deletion, L281L was used as a PCR template together with a BamHI-added forward primer and an XhoI-added reverse primer. The amplified fragments were digested with BamHI and XhoI and then inserted in the BglII-SalI sites of pEGFP-C1 (Clontech). N-terminus regions of Mbnl1, Mbnl2 and Mbnl3 were described previously (37). Constructs encoding an *Actn1* minigene and RFP-Bimax2 were described previously (35,37). A DMPK3′-N3 construct with CTG18, interrupted CTG480, interrupted CTG900 or interrupted CAG480 contained two terminal exons as well as the intervening intron of human *DMPK* gene, which were excised from RFP-DMPK3′ constructs (37) and inserted into pCMV-N3, a tag-less vector made by deleting the EGFP fragment from pEGFP-N3 (Clontech). The *Mbnl1* minigene fragment covering exon 6 to exon 8 was amplified from mouse genomic DNA by PCR using a primer set of BamHI-Mbnl1-ex6-Fw and SalI-Mbnl1-ex8-Rv, in which restriction sites for BamHI and SalI were added, respectively. These fragments were cleaved by BglII and the SalI and then subcloned into the BglII-SalI restriction sites of pEGFP-C1. Non-coding CAG or CTG repeat constructs were made by inserting interrupted repeat fragments into the XhoI site of pcDNA3.1 V5-His A, B or C (Invitrogen). Constructs for microRNA-based RNAi were described previously (37). miMbnl1-236 and miMbnl2-675 were used for knockdown of murine endogenous Mbnl1 and Mbnl2, respectively. For simultaneous knockdown of Mbnl1 and Mbnl2, miMbnl1-146 was utilized (37).

Cell culture and transfection

COS-7 and N2a cells were maintained in Dulbecco's modified Eagle's medium and 10% fetal bovine serum. For minigene assays, cells were typically cultured in 12-well plates and transfected with 0.5 μg of plasmids for protein expression (or cognate empty vector) and 10 or 20 ng of plasmids for the expression of a minigene using Lipofectamine 2000 (Invitrogen) according to the manufacturer's instructions. When multiple plasmids were transfected for protein expression, the total amount of plasmids was adjusted to 0.5 μg. For microscopic studies, cells were plated in 8-well chamber slides and transfected with 120 ng of plasmids in total. For subcellular localization studies, cells were plated in a 24-well or 96-well plate. The cell line expressing EGFP-MBNL1$_{40}$ (A6) was described previously (37). The following cell lines were obtained from the NIGMS Human Genetic Cell Repository at the Coriell Institute for Medical Research (GM04647:DM1000 and GM04795:control). StHdh cells were obtained from Dr Macdonald and CHDI through Coriell Institute. These cell lines were maintained as recommended by the supplier. We used FuGENE HD (Promega) diluted in OPTI-MEM (Invitrogen) for transfection of StHdh cells.

Cellular splicing assay

Cellular splicing assay was performed as previously described (37). For *Mbnl1* splicing, minigene fragments were amplified by PCR using a fluorescein isothiocyanate (FITC)-labeled forward primer for a 3′ region of EGFP sequence, FITC-GFP-Fw, and a gene-specific reverse primer, Mbnl1-splicing-Rv2. PCR products were resolved by 2.0–2.5% agarose gel electrophoresis. The fluorescence of PCR products was captured and visualized by LAS-1000 (FUJIFILM) or ImageQuant LAS 4000 (GE Healthcare Japan). Intensity of band signals was analyzed using Multigauge software (FUJIFILM).

Quantitative PCR

Gene-specific primers were designed using Primer Express software (Applied BioSystems) and are listed in Supplementary Material, Table S1. cDNA and gene-specific primer sets were mixed with Power SYBR Green PCR Master Mix (Applied BioSystems) or Fast Start Universal SYBR Green Master (Roche). Real-time amplification and quantification were performed using ABI7700 (Applied BioSystems) or LightCycler 480 II (Roche) following the manufacturer's protocol.

Fluorescence *in situ* hybridization

Fluorescence in situ hybridization was performed essentially as previously described with minor modifications (6,53). Cells plated in the 8-well chamber slides or 96-well plates were transfected using Lipofectamine 2000 (Invitrogen). Twenty-four hours post-transfection, cells were fixed with 4% paraformaldehyde–PBS for 0.5–1 h. Cells were treated for 5 min with 2% acetone–PBS pre-chilled at −30°C for permeabilization, followed by 10 min of pre-hybridization using 40% formamide–2× SSC solution. When necessary, DNase or RNase was treated before pre-hybridization. Hybridization mixture

contained 40% formamide, 2× SSC, vanadyl-nucleoside complex, BSA, yeast tRNA and 1 ng/ml (CTG)8 or (CAG)8 probe conjugated with Alexa-647 or -546. We also used Cy3-conjugated 2-O-methyl-modified RNA (CUG)8 or (CAG)8 probes at the same concentration. Hybridization was performed at 37°C for 2–3 h. After hybridization, cells were washed with 40% formamide–2× SSC and PBS. Cells were treated with Hoechst33342 (300 mg/ml) in PBS for 40 min to stain the nuclei followed by PBS wash three times. VECTASHIELD Mounting Medium (Vector Laboratories, Inc.) was used for mounting. Fluorescent images were obtained by sequential scan using a Leica TCS SP2 MP confocal microscope. 40× and 63× objectives were used. Obtained images were processed using Adobe Photoshop 5.5.

Subcellular localization analysis

Cells were plated on a 24-well or 96-well plate. Typically at 24 h after transfection, cells were fixed by 4% PFA–PBS containing Hoechst33342 for 0.5–1 h at room temperature followed by washing with PBS three times. In the case of repeat RNA localization analysis, FISH was performed using oligonucleotides labeled with Alexa-647, Alexa-546 or Cy3 (Supplementary Material, Table S1). Quantitative localization analysis was performed using ArrayScanVTI High Content Screening Reader (Cellomics) as previously described (35). An NCI was defined as (cytoplasmic intensity per pixel)/(cytoplasmic intensity per pixel + nuclear intensity per pixel). In one experiment, at least 150 cells were analyzed for each construct and the average NCI value of the cell population was calculated.

SUPPLEMENTARY MATERIAL

Supplementary Material is available at *HMG* online.

ACKNOWLEDGEMENTS

We thank Dr M. MacDonald and CHDI for StHdh cells and Ms Tomoko Yoda and Ms Itsuko Yamamoto for animal maintenance and the staff members of Research Resource Center at RIKEN Brain Science Institute for DNA sequencing and cell sorting. Y.K. was supported by the RIKEN Special Postdoctoral Researchers Program.

Conflict of Interest statement. None declared.

FUNDING

This work was supported by the Grant-in-Aid from the Ministry of Education, Culture, Sports, Science, and Technology of Japan to N.N. (22110004, 22240037, 24659436 and 25253066) and to Y.K. (19790620, 21790854, 23791007 and 25461299) and by a Grant-in-Aid for the Research on Measures for Ataxic Diseases from the Ministry of Health, Welfare and Labor to N.N.

REFERENCES

1. La Spada, A.R. and Taylor, J.P. (2010) Repeat expansion disease: progress and puzzles in disease pathogenesis. *Nat. Rev. Genet.*, **11**, 247–258.
2. DeJesus-Hernandez, M., Mackenzie, I.R., Boeve, B.F., Boxer, A.L., Baker, M., Rutherford, N.J., Nicholson, A.M., Finch, N.A., Flynn, H., Adamson, J. *et al.* (2011) Expanded GGGGCC hexanucleotide repeat in noncoding region of C9ORF72 causes chromosome 9p-linked FTD and ALS. *Neuron*, **72**, 245–256.
3. Kobayashi, H., Abe, K., Matsuura, T., Ikeda, Y., Hitomi, T., Akechi, Y., Habu, T., Liu, W., Okuda, H. and Koizumi, A. (2011) Expansion of intronic GGCCTG hexanucleotide repeat in NOP56 causes SCA36, a type of spinocerebellar ataxia accompanied by motor neuron involvement. *Am. J. Hum. Genet.*, **89**, 121–130.
4. Renton, A.E., Majounie, E., Waite, A., Simon-Sanchez, J., Rollinson, S., Gibbs, J.R., Schymick, J.C., Laaksovirta, H., van Swieten, J.C., Myllykangas, L. *et al.* (2011) A hexanucleotide repeat expansion in C9ORF72 is the cause of chromosome 9p21-linked ALS-FTD. *Neuron*, **72**, 257–268.
5. Liquori, C.L., Ricker, K., Moseley, M.L., Jacobsen, J.F., Kress, W., Naylor, S.L., Day, J.W. and Ranum, L.P. (2001) Myotonic dystrophy type 2 caused by a CCTG expansion in intron 1 of ZNF9. *Science*, **293**, 864–867.
6. Mankodi, A., Urbinati, C.R., Yuan, Q.P., Moxley, R.T., Sansone, V., Krym, M., Henderson, D., Schalling, M., Swanson, M.S. and Thornton, C.A. (2001) Muscleblind localizes to nuclear foci of aberrant RNA in myotonic dystrophy types 1 and 2. *Hum. Mol. Genet.*, **10**, 2165–2170.
7. Rudnicki, D.D., Holmes, S.E., Lin, M.W., Thornton, C.A., Ross, C.A. and Margolis, R.L. (2007) Huntington's disease-like 2 is associated with CUG repeat-containing RNA foci. *Ann. Neurol.*, **61**, 272–282.
8. Daughters, R.S., Tuttle, D.L., Gao, W., Ikeda, Y., Moseley, M.L., Ebner, T.J., Swanson, M.S. and Ranum, L.P. (2009) RNA gain-of-function in spinocerebellar ataxia type 8. *PLoS Genet.*, **5**, e1000600.
9. Kino, Y., Mori, D., Oma, Y., Takeshita, Y., Sasagawa, N. and Ishiura, S. (2004) Muscleblind protein, MBNL1/EXP, binds specifically to CHHG repeats. *Hum. Mol. Genet.*, **13**, 495–507.
10. Jiang, H., Mankodi, A., Swanson, M.S., Moxley, R.T. and Thornton, C.A. (2004) Myotonic dystrophy type 1 is associated with nuclear foci of mutant RNA, sequestration of muscleblind proteins and deregulated alternative splicing in neurons. *Hum. Mol. Genet.*, **13**, 3079–3088.
11. Lin, X., Miller, J.W., Mankodi, A., Kanadia, R.N., Yuan, Y., Moxley, R.T., Swanson, M.S. and Thornton, C.A. (2006) Failure of MBNL1-dependent post-natal splicing transitions in myotonic dystrophy. *Hum. Mol. Genet.*, **15**, 2087–2097.
12. Fardaei, M., Rogers, M.T., Thorpe, H.M., Larkin, K., Hamshere, M.G., Harper, P.S. and Brook, J.D. (2002) Three proteins, MBNL, MBLL and MBXL, co-localize in vivo with nuclear foci of expanded-repeat transcripts in DM1 and DM2 cells. *Hum. Mol. Genet.*, **11**, 805–814.
13. Kanadia, R.N., Johnstone, K.A., Mankodi, A., Lungu, C., Thornton, C.A., Esson, D., Timmers, A.M., Hauswirth, W.W. and Swanson, M.S. (2003) A muscleblind knockout model for myotonic dystrophy. *Science*, **302**, 1978–1980.
14. Kanadia, R.N., Shin, J., Yuan, Y., Beattie, S.G., Wheeler, T.M., Thornton, C.A. and Swanson, M.S. (2006) Reversal of RNA missplicing and myotonia after muscleblind overexpression in a mouse poly(CUG) model for myotonic dystrophy. *Proc. Natl. Acad. Sci. USA*, **103**, 11748–11753.
15. Chamberlain, C.M. and Ranum, L.P. (2012) Mouse model of muscleblind-like 1 overexpression: skeletal muscle effects and therapeutic promise. *Hum. Mol. Genet.*, **21**, 4645–4654.
16. Hao, M., Akrami, K., Wei, K., De Diego, C., Che, N., Ku, J.H., Tidball, J., Graves, M.C., Shieh, P.B. and Chen, F. (2008) Muscleblind-like 2 (Mbnl2)-deficient mice as a model for myotonic dystrophy. *Dev. Dyn.*, **237**, 403–410.
17. Charizanis, K., Lee, K.Y., Batra, R., Goodwin, M., Zhang, C., Yuan, Y., Shiue, L., Cline, M., Scotti, M.M., Xia, G. *et al.* (2012) Muscleblind-like 2-mediated alternative splicing in the developing brain and dysregulation in myotonic dystrophy. *Neuron*, **75**, 437–450.
18. Bauer, P.O. and Nukina, N. (2009) The pathogenic mechanisms of polyglutamine diseases and current therapeutic strategies. *J. Neurochem.*, **110**, 1737–1765.
19. Moseley, M.L., Zu, T., Ikeda, Y., Gao, W., Mosemiller, A.K., Daughters, R.S., Chen, G., Weatherspoon, M.R., Clark, H.B., Ebner, T.J. *et al.* (2006) Bidirectional expression of CUG and CAG expansion transcripts and intranuclear polyglutamine inclusions in spinocerebellar ataxia type 8. *Nat. Genet.*, **38**, 758–769.
20. Wilburn, B., Rudnicki, D.D., Zhao, J., Weitz, T.M., Cheng, Y., Gu, X., Greiner, E., Park, C.S., Wang, N., Sopher, B.L. *et al.* (2011) An antisense

CAG repeat transcript at JPH3 locus mediates expanded polyglutamine protein toxicity in Huntington's disease-like 2 mice. *Neuron*, **70**, 427–440.
21. Zu, T., Gibbens, B., Doty, N.S., Gomes-Pereira, M., Huguet, A., Stone, M.D., Margolis, J., Peterson, M., Markowski, T.W., Ingram, M.A. *et al.* (2011) Non-ATG-initiated translation directed by microsatellite expansions. *Proc. Natl. Acad. Sci. USA*, **108**, 260–265.
22. Li, L.B., Yu, Z., Teng, X. and Bonini, N.M. (2008) RNA toxicity is a component of ataxin-3 degeneration in Drosophila. *Nature*, **453**, 1107–1111.
23. Hsu, R.J., Hsiao, K.M., Lin, M.J., Li, C.Y., Wang, L.C., Chen, L.K. and Pan, H. (2011) Long tract of untranslated CAG repeats is deleterious in transgenic mice. *PLoS One*, **6**, e16417.
24. Mykowska, A., Sobczak, K., Wojciechowska, M., Kozlowski, P. and Krzyzosiak, W.J. (2011) CAG repeats mimic CUG repeats in the misregulation of alternative splicing. *Nucl. Acids Res.*, **39**, 8938–8951.
25. Wang, L.C., Chen, K.Y., Pan, H., Wu, C.C., Chen, P.H., Liao, Y.T., Li, C., Huang, M.L. and Hsiao, K.M. (2011) Muscleblind participates in RNA toxicity of expanded CAG and CUG repeats in *Caenorhabditis elegans*. *Cell Mol. Life Sci.*, **68**, 1255–1267.
26. Ho, T.H., Savkur, R.S., Poulos, M.G., Mancini, M.A., Swanson, M.S. and Cooper, T.A. (2005) Colocalization of muscleblind with RNA foci is separable from mis-regulation of alternative splicing in myotonic dystrophy. *J. Cell Sci.*, **118**, 2923–2933.
27. Yuan, Y., Compton, S.A., Sobczak, K., Stenberg, M.G., Thornton, C.A., Griffith, J.D. and Swanson, M.S. (2007) Muscleblind-like 1 interacts with RNA hairpins in splicing target and pathogenic RNAs. *Nucl. Acids Res.*, **35**, 5474–5486.
28. Dhaenens, C.M., Schraen-Maschke, S., Tran, H., Vingtdeux, V., Ghanem, D., Leroy, O., Delplanque, J., Vanbrussel, E., Delacourte, A., Vermersch, P. *et al.* (2008) Overexpression of MBNL1 fetal isoforms and modified splicing of Tau in the DM1 brain: two individual consequences of CUG trinucleotide repeats. *Exp. Neurol.*, **210**, 467–478.
29. Gates, D.P., Coonrod, L.A. and Berglund, J.A. (2011) Autoregulated splicing of muscleblind-like 1 (MBNL1) Pre-mRNA. *J. Biol. Chem.*, **286**, 34224–34233.
30. Fernandez-Costa, J.M. and Artero, R. (2010) A conserved motif controls nuclear localization of *Drosophila Muscleblind*. *Mol. Cells*, **30**, 65–70.
31. Tran, H., Gourrier, N., Lemercier-Neuillet, C., Dhaenens, C.M., Vautrin, A., Fernandez-Gomez, F.J., Arandel, L., Carpentier, C., Obriot, H., Eddarkaoui, S. *et al.* (2011) Analysis of exonic regions involved in nuclear localization, splicing activity, and dimerization of Muscleblind-like-1 isoforms. *J. Biol. Chem.*, **286**, 16435–16446.
32. Dansithong, W., Paul, S., Comai, L. and Reddy, S. (2005) MBNL1 is the primary determinant of focus formation and aberrant insulin receptor splicing in DM1. *J. Biol. Chem.*, **280**, 5773–5780.
33. Smith, K.P., Byron, M., Johnson, C., Xing, Y. and Lawrence, J.B. (2007) Defining early steps in mRNA transport: mutant mRNA in myotonic dystrophy type I is blocked at entry into SC-35 domains. *J. Cell Biol.*, **178**, 951–964.
34. Querido, E., Gallardo, F., Beaudoin, M., Menard, C. and Chartrand, P. (2011) Stochastic and reversible aggregation of mRNA with expanded CUG-triplet repeats. *J. Cell Sci.*, **124**, 1703–1714.
35. Kino, Y., Washizu, C., Aquilanti, E., Okuno, M., Kurosawa, M., Yamada, M., Doi, H. and Nukina, N. (2011) Intracellular localization and splicing regulation of FUS/TLS are variably affected by amyotrophic lateral sclerosis-linked mutations. *Nucl. Acids Res.*, **39**, 2781–2798.
36. Gromak, N., Matlin, A.J., Cooper, T.A. and Smith, C.W. (2003) Antagonistic regulation of alpha-actinin alternative splicing by CELF proteins and polypyrimidine tract binding protein. *RNA*, **9**, 443–456.
37. Kino, Y., Washizu, C., Oma, Y., Onishi, H., Nezu, Y., Sasagawa, N., Nukina, N. and Ishiura, S. (2009) MBNL and CELF proteins regulate alternative splicing of the skeletal muscle chloride channel CLCN1. *Nucl. Acids Res.*, **37**, 6477–6490.
38. Kosugi, S., Hasebe, M., Entani, T., Takayama, S., Tomita, M. and Yanagawa, H. (2008) Design of peptide inhibitors for the importin alpha/beta nuclear import pathway by activity-based profiling. *Chem. Biol.*, **15**, 940–949.
39. Chook, Y.M. and Suel, K.E. (2011) Nuclear import by karyopherin-betas: recognition and inhibition. *Biochim. Biophys. Acta.*, **1813**, 1593–1606.
40. Terenzi, F. and Ladd, A.N. (2010) Conserved developmental alternative splicing of muscleblind-like (MBNL) transcripts regulates MBNL localization and activity. *RNA Biol.*, **7**, 43–55.
41. Lee, K.Y., Li, M., Manchanda, M., Batra, R., Charizanis, K., Mohan, A., Warren, S.A., Chamberlain, C.M., Finn, D., Hong, H. *et al.* (2013) Compound loss of muscleblind-like function in myotonic dystrophy. *EMBO Mol. Med.*, **5**, 1887–1900.
42. Adereth, Y., Dammai, V., Kose, N., Li, R. and Hsu, T. (2005) RNA-dependent integrin alpha3 protein localization regulated by the Muscleblind-like protein MLP1. *Nat. Cell Biol.*, **7**, 1240–1247.
43. Wang, E.T., Cody, N.A., Jog, S., Biancolella, M., Wang, T.T., Treacy, D.J., Luo, S., Schroth, G.P., Housman, D.E., Reddy, S. *et al.* (2012) Transcriptome-wide regulation of pre-mRNA splicing and mRNA localization by muscleblind proteins. *Cell*, **150**, 710–724.
44. de Mezer, M., Wojciechowska, M., Napierala, M., Sobczak, K. and Krzyzosiak, W.J. (2011) Mutant CAG repeats of Huntingtin transcript fold into hairpins, form nuclear foci and are targets for RNA interference. *Nucl. Acids Res.*, **39**, 3852–3863.
45. Oma, Y., Kino, Y., Sasagawa, N. and Ishiura, S. (2005) Comparative analysis of the cytotoxicity of homopolymeric amino acids. *Biochim. Biophys. Acta.*, **1748**, 174–179.
46. Wheeler, T.M., Leger, A.J., Pandey, S.K., MacLeod, A.R., Nakamori, M., Cheng, S.H., Wentworth, B.M., Bennett, C.F. and Thornton, C.A. (2012) Targeting nuclear RNA for in vivo correction of myotonic dystrophy. *Nature*, **488**, 111–115.
47. Ash, P.E., Bieniek, K.F., Gendron, T.F., Caulfield, T., Lin, W.L., Dejesus-Hernandez, M., van Blitterswijk, M.M., Jansen-West, K., Paul, J.W. 3rd, Rademakers, R. *et al.* (2013) Unconventional translation of C9ORF72 GGGGCC expansion generates insoluble polypeptides specific to c9FTD/ALS. *Neuron*, **77**, 639–646.
48. Mori, K., Arzberger, T., Grasser, F.A., Gijselinck, I., May, S., Rentzsch, K., Weng, S.M., Schludi, M.H., van der Zee, J., Cruts, M. *et al.* (2013) Bidirectional transcripts of the expanded C9orf72 hexanucleotide repeat are translated into aggregating dipeptide repeat proteins. *Acta. Neuropathol.*, **126**, 881–893.
49. Mori, K., Weng, S.M., Arzberger, T., May, S., Rentzsch, K., Kremmer, E., Schmid, B., Kretzschmar, H.A., Cruts, M., Van Broeckhoven, C. *et al.* (2013) The C9orf72 GGGGCC repeat is translated into aggregating dipeptide-repeat proteins in FTLD/ALS. *Science*, **339**, 1335–1338.
50. Todd, P.K., Oh, S.Y., Krans, A., He, F., Sellier, C., Frazer, M., Renoux, A.J., Chen, K.C., Scaglione, K.M., Basrur, V. *et al.* (2013) CGG repeat-associated translation mediates neurodegeneration in fragile X tremor ataxia syndrome. *Neuron*, **78**, 440–455.
51. Zu, T., Liu, Y., Banez-Coronel, M., Reid, T., Pletnikova, O., Lewis, J., Miller, T.M., Harms, M.B., Falchook, A.E., Subramony, S.H. *et al.* (2013) RAN proteins and RNA foci from antisense transcripts in C9ORF72 ALS and frontotemporal dementia. *Proc. Natl. Acad. Sci. USA*, **110**, E4968–E4977.
52. Gendron, T.F., Bieniek, K.F., Zhang, Y.J., Jansen-West, K., Ash, P.E., Caulfield, T., Daughrity, L., Dunmore, J.H., Castanedes-Casey, M., Chew, J. *et al.* (2013) Antisense transcripts of the expanded C9ORF72 hexanucleotide repeat form nuclear RNA foci and undergo repeat-associated non-ATG translation in c9FTD/ALS. *Acta Neuropathol.*, **126**, 829–844.
53. Fardaei, M., Larkin, K., Brook, J.D. and Hamshere, M.G. (2001) In vivo co-localisation of MBNL protein with DMPK expanded-repeat transcripts. *Nucl. Acids Res.*, **29**, 2766–2771.

Human Molecular Genetics, 2015, Vol. 24, No. 4 **1092–1105**
doi:10.1093/hmg/ddu522
Advance Access published on October 9, 2014

Depletion of p62 reduces nuclear inclusions and paradoxically ameliorates disease phenotypes in Huntington's model mice

Masaru Kurosawa[3,4,5,8], Gen Matsumoto[1,4,5,8], Yoshihiro Kino[1,4,5,8], Misako Okuno[4], Mizuki Kurosawa-Yamada[4], Chika Washizu[4], Harumi Taniguchi[1,4,5], Kazuhiro Nakaso[6], Toru Yanagawa[7], Eiji Warabi[7], Tomomi Shimogori[5], Takashi Sakurai[3], Nobutaka Hattori[2] and Nobuyuki Nukina[1,4,5,8,*]

[1]Department of Neuroscience for Neurodegenerative Disorders, [2]Department of Neurology, [3]Department of Cellular and Molecular Pharmacology, Juntendo University Graduate School of Medicine, Tokyo 113-8421, Japan, [4]Laboratory for Structural Neuropathology, [5]Laboratory for Molecular Mechanisms of Thalamus Development, RIKEN Brain Science Institute, Saitama 351-0198, Japan, [6]Department of Neurology, Institute of Neurological Sciences, Faculty of Medicine, Tottori University, Tottori 683-8504, Japan, [7]Faculty of Medicine, University of Tsukuba, 1-1-1 Tennoudai, Tsukuba 305-8575, Japan and [8]CREST (Core Research for Evolutionary Science and Technology), JST, Tokyo 102-0076, Japan

Received September 9, 2014; Revised and Accepted October 7, 2014

Huntington's disease (HD) is a dominantly inherited genetic disease caused by mutant huntingtin (htt) protein with expanded polyglutamine (polyQ) tracts. A neuropathological hallmark of HD is the presence of neuronal inclusions of mutant htt. p62 is an important regulatory protein in selective autophagy, a process by which aggregated proteins are degraded, and it is associated with several neurodegenerative disorders including HD. Here, we investigated the effect of p62 depletion in three HD model mice: R6/2, HD190QG and HD120QG mice. We found that loss of p62 in these models led to longer life spans and reduced nuclear inclusions, although cytoplasmic inclusions increased with polyQ length. In mouse embryonic fibroblasts (MEFs) with or without p62, mutant htt with a nuclear localization signal (NLS) showed no difference in nuclear inclusion between the two MEF types. In the case of mutant htt without NLS, however, p62 depletion increased cytoplasmic inclusions. Furthermore, to examine the effect of impaired autophagy in HD model mice, we crossed R6/2 mice with *Atg5* conditional knockout mice. These mice also showed decreased nuclear inclusions and increased cytoplasmic inclusions, similar to HD mice lacking p62. These data suggest that the genetic ablation of p62 in HD model mice enhances cytoplasmic inclusion formation by interrupting autophagic clearance of polyQ inclusions. This reduces polyQ nuclear influx and paradoxically ameliorates disease phenotypes by decreasing toxic nuclear inclusions.

INTRODUCTION

Intracellular protein aggregation is a main feature of many neurodegenerative disorders such as tauopathies, synucleinopaties, TDP-43 proteinopathies and polyglutamine (polyQ) diseases (1). In these pathological conditions, misfolded proteins, which are ubiquitinated, accumulate as cytoplasmic or nuclear inclusions. PolyQ diseases, one of the most common inherited types of neurodegenerative disorders, are based on CAG-repeat expansions and their gene products, expanded polyQ proteins. Expanded polyQ proteins are misfolded, and when deposited in the nucleus, they may sequester transcription factors and other molecules that induce further pathological processes and neuronal degeneration (2).

The misfolded proteins are degraded through two main routes for eukaryotic intracellular protein clearance, the ubiquitin–proteasome system (UPS) and the autophagy–lysosome pathway. The UPS is essential in regulating many cellular processes, including cell division, signal transduction and gene expression. Proteasomes degrade substrates that are covalently

*To whom correspondence should be addressed. Tel: +81 70 6969 1951; Fax: +81 3 5800 0547; Email: nnukina@juntendo.ac.jp

linked with ubiquitin by an ubiquitin-conjugating system composed of E1 (ubiquitin-activating enzyme), E2 (ubiquitin-conjugating enzyme) and E3 (ubiquitin ligase). This system also ubiquitinates misfolded proteins, but misfolded proteins have a strong tendency to form inclusions that cannot be degraded by a proteasome. Macroautophagy is another degradation mechanism responsible for degradation of long-lived proteins and entire organelles. In this system, organelles and protein inclusions are surrounded by double-membraned autophagosomes, which fuse with a lysosome to degrade their contents by a rather non-selective, bulk degradation. However, another type of autophagic degradation called selective autophagy involves ubiquitin and ubiquitin-binding proteins such as p62 (3).

We previously reported that p62 is a protein that interacts with polyQ aggregates and is induced by expanded polyQ expression, suggesting that p62 is a stress-responsive protein induced by polyQ expression and proteasomal inhibition (4). p62 is also a common component of neuronal protein inclusions in neurodegenerative diseases in humans and model mice (4–8). p62 is well known as an adaptor protein that has multiple roles in the activation of the transcription factor NF-kappa B, tumorigenesis and osteoclastogenesis. p62 was recently reported to play an important role in the selective autophagy of ubiquitinated proteins. Autophagy-deficient *ATG5* or *7* knockout mice showed ubiquitin-positive inclusions (9,10) that disappeared after *p62* was knocked out, suggesting that p62 could play a role in controlling intracellular inclusion body formation (11).

It was reported that autophagy inhibition increases the level of soluble UPS client proteins by slowing their clearance. This was closely associated with the accumulation of p62 (12). Furthermore, *p62* knockdown in autophagy-deficient cells normalizes levels of UPS clients. From these results, p62 was suggested to be a key protein in regulating protein aggregate formation, especially in autophagy-deficient conditions. However, it remains unclear whether the decrease in p62 is beneficial or detrimental, particularly *in vivo*. A previous report shows that genetic inactivation of *p62* in mice leads to accumulation of hyperphosphorylated tau and neurodegeneration (13). In polyQ diseases, the inclusions are mainly observed in the nuclei, where autophagy cannot work. Little is known, however, about the effect of *p62* knockout for polyQ diseases *in vivo*. In this report, we observed the cytoplasmic accumulation of polyQ inclusions and the decrease of nuclear inclusions in polyQ model mice with the loss of p62. The detailed mechanism was investigated, in comparison with the effects of *Atg5* knockout.

RESULTS

Paradoxical decrease of nuclear inclusion formation in polyQ model mice lacking *p62*

We first investigated pathological changes in R6/2 mice with or without *p62*. Anti-huntingtin (htt) antibody (EM48) revealed fewer and smaller nuclear inclusions in the brains of R6/2;$p62^{-/-}$ compared with those of R6/2;$p62^{-/+}$ or R6/2;$p62^{+/+}$ mice starting at 4 weeks of age (Fig. 1A and Supplementary Material, Fig. S1). Immunofluorescent staining of hippocampal CA1 revealed that the proportion of nuclei with inclusions in R6/2;$p62^{-/-}$ mice was significantly lower than that in R6/2;$p62^{+/+}$ or R6/2;$p62^{-/+}$ mice at each age (Fig. 1B). The average size of these nuclear inclusions became larger with age, and the inclusions in R6/2;$p62^{-/-}$ mice grew at a slower rate than those in R6/2;$p62^{+/+}$ or R6/2;$p62^{-/+}$ mice (Fig. 1C and Supplementary Material, Fig. S2). To clearly distinguish nuclear from cytoplasmic inclusions, we stained nuclear membranes with anti-Lamin B antibody (Fig. 1D).

Next, we investigated the distribution of inclusions in the striatum, which is the most affected region in HD, in R6/2;*p62* and HD190QG;p62 mice (Fig. 2). In R6/2;*p62* mice, anti-htt antibody (EM48) revealed significantly fewer nuclear inclusions and significantly more cytoplasmic inclusions in R6/2;$p62^{-/-}$ versus R6/2;$p62^{+/+}$ mice starting at 4 weeks of age (Fig. 2A, C and D). In HD190QG;*p62* mice, anti-htt antibody (EM48) revealed significantly fewer nuclear inclusions in HD190QG;$p62^{-/-}$ versus HD190QG;$p62^{+/+}$ mice starting at 8 weeks of age (Fig. 2E, G and H); there were significantly more cytoplasmic inclusions in HD190QG;$p62^{-/-}$ versus HD190QG;$p62^{+/+}$ mice from 8 to 16 weeks of age (Fig. 2E and H). At 24 weeks, although there was no significant difference in the number of the cytoplasmic inclusions, the size of cytoplasmic inclusions was greater in HD190QG;$p62^{-/-}$ versus HD190QG;$p62^{+/+}$ mice (Fig. 2I). To clearly distinguish nuclear from cytoplasmic inclusions, we stained nuclear membranes with anti-Lamin B antibody (Fig. 2B and F). The expression level of mutant htt mRNA was similar in R6/2;$p62^{+/+}$ and R6/2;$p62^{-/-}$ mice, and p62 expression was not affected by the htt transgene (Supplementary Material, Fig. S3).

When we examined the distribution of inclusions in the hippocampus, we could clearly see an increase in cytoplasmic or neuropil inclusions, especially in stratum radiatum (arrowheads) of the hippocampus of R6/2;$p62^{-/-}$ mice (Fig. 3A). Double immunofluorescence staining with anti-htt (N-18) and anti-MAP2 antibodies (dendritic marker) showed that part of those inclusions was localized in dendrites in the stratum radiatum of R6/2;$p62^{-/-}$ mice (Fig. 3B, lower panel). On the other hand, in the stratum radiatum of R6/2;$p62^{+/+}$ mice, inclusions were seen in the nuclei but not in dendrites (Fig. 3B, upper panel). We further analyzed HD190QG mice, in which GFP-positive cytoplasmic inclusions are clearly observed. In HD190QG;$p62^{-/-}$ mice, we observed a greater number of neuropil inclusions in the molecular layer of the dentate gyrus (MolDG; arrows) as well as striatum radiatum (Rad; arrowheads) compared with HD190QG;$p62^{+/+}$ mice (Fig. 3C). The inclusions in the lacunosum molecular layer (LMol) of HD190QG;$p62^{+/+}$ mice increased with age, but this was not observed in HD190QG;$p62^{-/-}$ mice. There were fewer inclusions in the hilus of dentate gyrus in HD190QG;$p62^{-/-}$ compared with HD190QG;$p62^{+/+}$ mice at each age. Those inclusions are in the dendrites (data not shown); however, we could not reveal why this change occurred. Further investigation is necessary. Double immunofluorescence staining with anti-GFP and anti-MAP2 antibodies showed that part of those inclusions was localized in dendrites (Fig. 3D). The dendrites of CA1 pyramidal neurons are distributed throughout Rad and LMol, and the dendrites of dentate granule cells are distributed throughout MolDG, suggesting that the dendritic inclusions increased in both neurons and shifted to proximal dendrites in the case of pyramidal neurons.

We then examined whether or not the insoluble htt fragment increased by using immunoblotting to confirm the immunohistochemistry results. We used the HD190QG line because it is difficult to consistently find the htt exon 1 fragment without a tag in

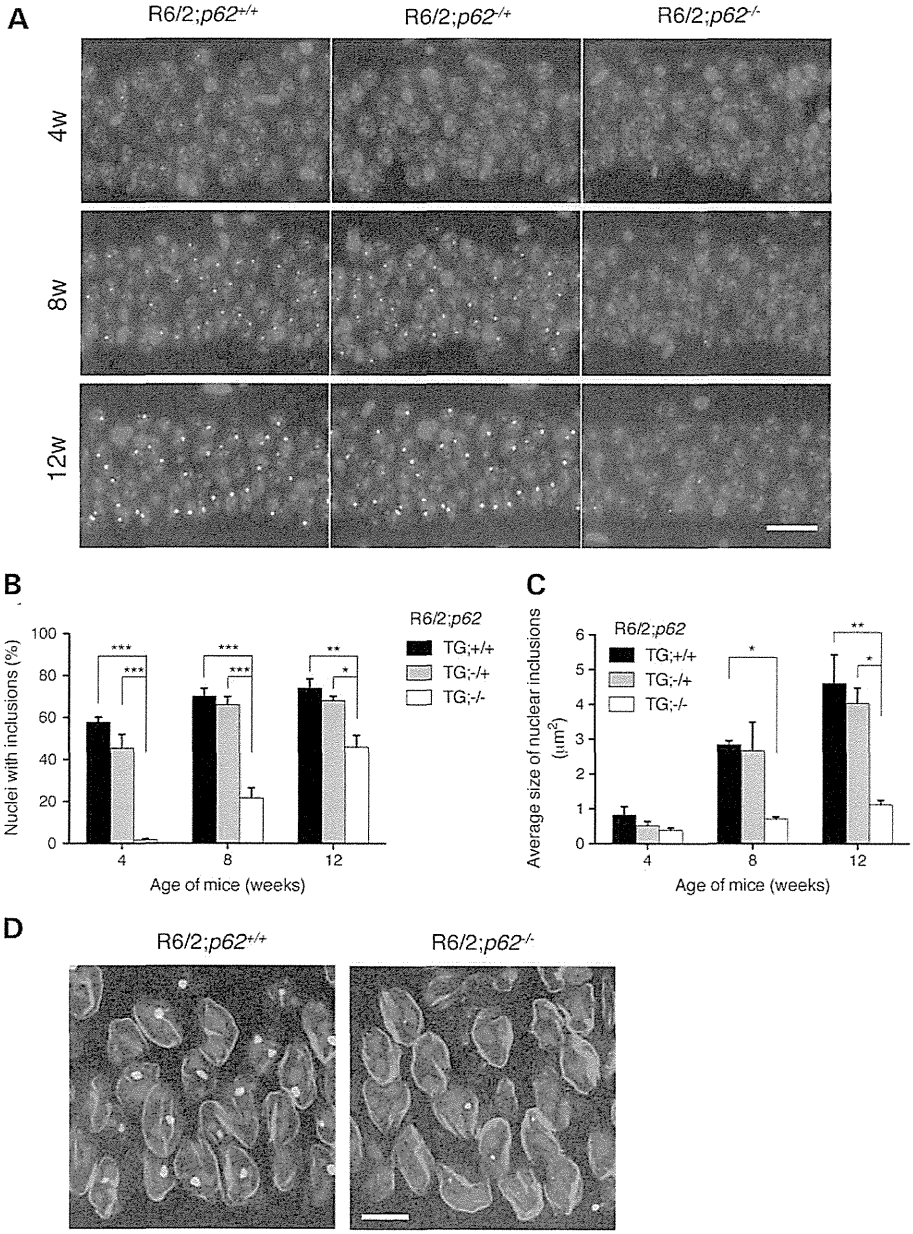

Figure 1. *p62* knockout reduced both the size and the number of the nuclear inclusions in R6/2 mice. (**A**) The hippocampal CA1 of R6/2 mice with and without *p62* was stained with anti-htt antibody (EM48) (−/−: knockout; −/+: hetero; +/+: wild littermates). (**B**) The percentage of nuclei with inclusions, analyzed by fluorescent immunostaining of the hippocampal CA1 with EM48. (**C**) The average size of nuclear inclusion in the hippocampal CA1. This size in R6/2;$p62^{-/-}$ was significantly smaller than in R6/2;$p62^{+/+}$ and R6/2;$p62^{-/+}$ at 12 weeks of age. (**D**) The hippocampal CA1 of R6/2;$p62^{+/+}$ and R6/2;$p62^{-/-}$ was stained with EM48 and a nuclear membrane marker, Lamin B, to clearly show the nuclear inclusions. Values are means ± SEM. ($^{*}P < 0.05$, $^{**}P < 0.01$, $^{***}P < 0.001$), (B and C). $n = 3$ for each genotype (B and C). Images were captured with BZ-9000 (A) and TCS SP5 (D). Nuclei were stained with DAPI (A and D). Scale bar = 30 μm (A) and 10 μm (D).

SDS–PAGE, as when R6/2 brain homogenates were examined, p62 was absent in HD190QG;$p62^{-/-}$ mice (Fig. 4A). In the total fraction, the soluble htt-enhanced green fluorescent protein (EGFP) band showed no obvious difference between HD190QG;$p62^{+/+}$ and HD190QG;$p62^{-/-}$ mice. Diffuse stainings and gel top stainings with anti-ubiquitin antibody also showed no obvious difference between HD190QG;$p62^{-/-}$ and HD190QG;$p62^{+/+}$ mice. Using the agarose gel electrophoresis for resolving aggregates (AGERA) method (14), which shows htt protein complexes with high molecular weight, we did not observe a definite difference between the htt protein complexes in the total fraction from HD190QG;$p62^{-/-}$ versus HD190QG;$p62^{+/+}$ mice (Fig. 4B). When the nuclear fraction was separated, however, HD190QG;$p62^{-/-}$ mice showed a decrease in htt protein

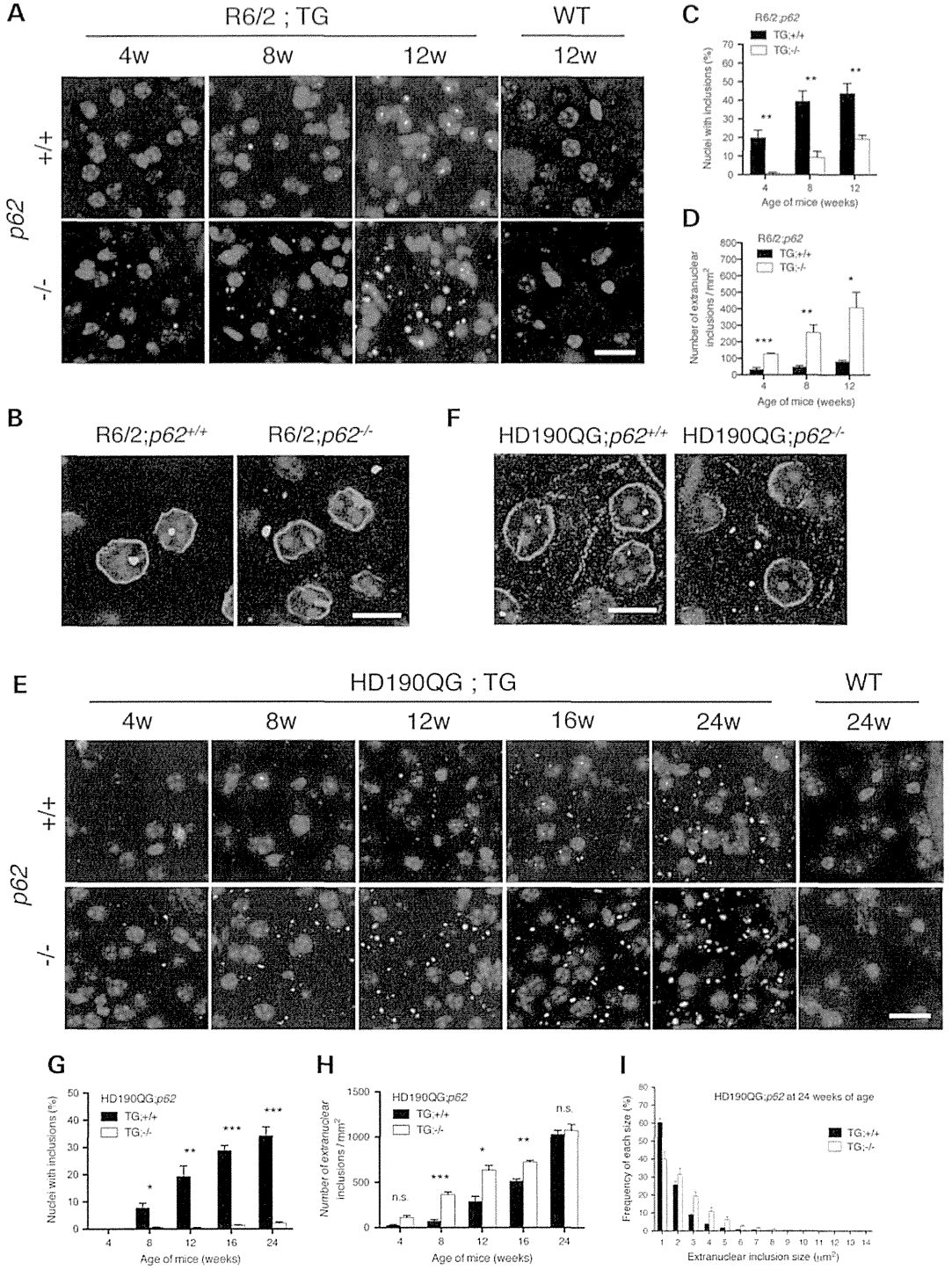

Figure 2. *p62* knockout reduced nuclear inclusions and increased extranuclear inclusions in the striatum in two different HD model mice. (**A**) The striatum of R6/2;$p62^{+/+}$ and R6/2;$p62^{-/-}$ mice was stained with anti-htt antibody (EM48). (**B**) The striatum of R6/2;$p62^{+/+}$ and R6/2;$p62^{-/-}$ mice was stained with EM48 and a nuclear membrane marker, Lamin B, to clearly show the nuclear inclusions. (**C** and **D**) The percentage of nuclei with inclusions (C) and the number of extranuclear inclusions (D) in the striatum of R6/2;$p62^{+/+}$ and R6/2;$p62^{-/-}$ mice, analyzed by fluorescent immunostaining with EM48. (**E**) The striatum of HD190QG;$p62^{+/+}$ and HD190QG;$p62^{-/-}$ mice was stained with EM48. (**F**) The striatum of HD190QG;$p62^{+/+}$ and HD190QG;$p62^{-/-}$ mice was stained with EM48 and a nuclear membrane marker, Lamin B, to clearly show the nuclear inclusions. (**G** and **H**) The percentage of nuclei with inclusions (G) and the number of the extranuclear inclusions (H) in the striatum of HD190QG;$p62^{+/+}$ and HD190QG;$p62^{-/-}$ mice, analyzed by fluorescent immunostaining with EM48. (**I**) Distribution of the size of extranuclear inclusions stained with anti-GFP antibody at 24 weeks of age. Values are means ± SEM. ($^{*}P < 0.05$, $^{**}P < 0.01$, $^{***}P < 0.001$), (C, D, G and H). $n = 3$ for each genotype (C, D, G, H and I). Images were captured with BZ-9000 (A and E) and TCS SP5 (B and F). Nuclei were stained with DAPI. Scale bar = 20 μm (A and E) and 10 μm (B and F).